AEDC-TR-77-115

INTEGRAL ANALYSIS OF DUCTED TWO-STREAM MIXING WITH RECIRCULATION

C. E. Peters and W. J. Phares
ARO, Inc., a Sverdrup Corporation Company

ENGINE TEST FACILITY
ARNOLD ENGINEERING DEVELOPMENT CENTER
AIR FORCE SYSTEMS COMMAND
ARNOLD AIR FORCE STATION, TENNESSEE 37389

March 1978

Final Report for Period October 1, 1976 – September 30, 1977

Prepared for

ARNOLD ENGINEERING DEVELOPMENT CENTER/DOT
ARNOLD AIR FORCE STATION, TENNESSEE 37389

NOTICES

When U. S. Government drawings, specifications, or other data are used for any purpose other than a definitely related Government procurement operation, the Government thereby incurs no responsibility nor any obligation whatsoever, and the fact that the Government may have formulated, furnished, or in any way supplied the said drawings, specifications, or other data, is not to be regarded by implication or otherwise, or in any manner licensing the holder or any other person or corporation, or conveying any rights or permission to manufacture, use, or sell any patented invention that may in any way be related thereto.

Qualified users may obtain copies of this report from the Defense Documentation Center.

References to named commerical products in this report are not to be considered in any sense as an indorsement of the product by the United States Air Force or the Government.

This report has been reviewed by the Information Office (OI) and is releasable to the National Technical Information Service (NTIS). At NTIS, it will be available to the general public, including foreign nations.

APPROVAL STATEMENT

This report has been reviewed and approved.

Elton R. Thompson

ELTON R. THOMPSON
Project Manager, Research Division
Directorate of Test Engineering

Approved for publication:

FOR THE COMMANDER

Marion L. Laster

MARION L. LASTER
Director of Test Engineering
Deputy for Operations

REPORT DOCUMENTATION PAGE		READ INSTRUCTIONS BEFORE COMPLETING FORM
1 REPORT NUMBER AEDC-TR-77-115	2. GOVT ACCESSION NO.	3. RECIPIENT'S CATALOG NUMBER
4. TITLE (and Subtitle) INTEGRAL ANALYSIS OF DUCTED TWO-STREAM MIXING WITH RECIRCULATION		5 TYPE OF REPORT & PERIOD COVERED Final Report - Oct 1, 1976 to Sept 30, 1977 6. PERFORMING ORG. REPORT NUMBER
7. AUTHOR(s) C. E. Peters and W. J. Phares, ARO, Inc.		8 CONTRACT OR GRANT NUMBER(s)
9 PERFORMING ORGANIZATION NAME AND ADDRESS Arnold Engineering Development Center/DOT Air Force Systems Command Arnold Air Force Station, TN 37389		10. PROGRAM ELEMENT, PROJECT, TASK AREA & WORK UNIT NUMBERS Program Element 65807F
11 CONTROLLING OFFICE NAME AND ADDRESS Arnold Engineering Development Center/DOS Arnold Air Force Station Tennessee 37389		12. REPORT DATE March 1978 13. NUMBER OF PAGES 69
14 MONITORING AGENCY NAME & ADDRESS(if different from Controlling Office)		15. SECURITY CLASS. (of this report) UNCLASSIFIED 15a. DECLASSIFICATION/DOWNGRADING SCHEDULE N/A

16 DISTRIBUTION STATEMENT (of this Report)

Approved for public release; distribution unlimited.

17. DISTRIBUTION STATEMENT (of the abstract entered in Block 20, if different from Report)

18 SUPPLEMENTARY NOTES

Available in DDC

19 KEY WORDS (Continue on reverse side if necessary and identify by block number)

analytical studies
mathematical analysis
mixing
ducted mixing system
recirculation
computers
mathematical models

20 ABSTRACT (Continue on reverse side if necessary and identify by block number)

The integral boundary-layer equations are used to develop an analysis of ducted turbulent mixing of coaxial streams. Non-recirculating flows, as well as flows with a recirculation region along the duct wall, are considered in the formulation. The flow geometry considered is either axisymmetric or planar, and provision is made to calculate flows with a centerbody. Chemical reactions in the mixing process, if they occur, are assumed to

DD FORM 1 JAN 73 1473 EDITION OF 1 NOV 65 IS OBSOLETE

20. ABSTRACT (Continued)

be in equilibrium. A simple eddy viscosity model is used to describe the turbulent transport processes. Comparison of the analytical results with experiments indicates that the location and extent of recirculation are well predicted, at least for flows with moderate density gradients. However, because of the neglect of streamwise turbulent transport processes in the analysis, the predicted concentration field in recirculating flow is in only fair agreement with experiment. An extended integral analysis, in which the streamwise turbulent transport of momentum and species is included in an approximate manner, is formulated.

AFSC
Arnold AFS Tenn

PREFACE

The work reported herein was conducted by the Arnold Engineering Development Center (AEDC), Air Force Systems Command (AFSC), under Program Element 65807F. The results presented were obtained by ARO, Inc., AEDC Division (a Sverdrup Corporation Company), operating contractor for the AEDC, AFSC, Arnold Air Force Station, Tennessee. The work was done under ARO Project Number R33A-03A. The manuscript was submitted for publication on October 28, 1977.

CONTENTS

ILLUSTRATIONS

Figure

Figure Page

APPENDIXES

1.0 INTRODUCTION

The turbulent mixing of two streams inside a duct occurs in many devices of interest to the engineer. Typical examples are jet pumps, composite propulsion systems such as air-augmented rockets, and various low-speed combustors. The flow field within engine test cells often involves the mixing of a high-speed exhaust jet with a low-speed secondary flow. In many applications, one must consider the occurrence of exothermic chemical reactions in the mixing process. And some flows, with low-speed secondary streams, have regions of recirculating flow along the duct wall.

Ducted flows without recirculation (Fig. 1a) can be accurately predicted by solving the boundary-layer equations, in which lateral pressure gradients are neglected and the velocity gradients in the lateral direction are assumed to be much larger than those in the axial direction. After the specification of a semi-empirical model for the turbulent transport of momentum, energy, and mass, the boundary-layer equations can be solved by finite-difference methods (e.g., Ref. 1) or by integral methods (e.g., Refs. 2 - 6).

In the duct flow field without recirculation, the axial velocity components are directed downstream throughout the entire flow. However, if the initial velocity of the secondary stream is very low compared with that of the primary stream, then a recirculation zone can occur along the duct wall (Fig. 1b). If the entire secondary flow is entrained by the mixing layer before the mixing layer propagates to the duct wall, then recirculation must occur to satisfy the requirement for additional mixing layer entrainment.

Experimental investigations, such as that of Barchilon and Curtet (Ref. 7), have identified the main features of ducted flows with recirculation. The wall static pressure gradually rises between the duct entrance and the front stagnation point (FSP), which is the station at which recirculation begins (Fig. 1b). The wall static pressure then remains nearly constant between the FSP and the station where the outer edge of the shear layer reaches the wall (Note that the edges of the shear layer are somewhat arbitrarily defined). Downstream of this station, which is the beginning of the reattachment region, the wall static pressure rises rapidly. In addition, the reverse-flow velocities along the wall, which are largest at the onset of reattachment, decrease quickly in the reattachment region and become zero at the rear stagnation point (RSP). Downstream of the RSP, the axial velocity components are everywhere positive, and the flow eventually becomes a fully developed pipe flow.

The experiments indicate that the reversed flow, between the edge of the shear layer and the duct wall, is highly turbulent and well stirred. Therefore, the flow in this region is nearly one-dimensional, with small gradients in the axial velocity and species profiles.

In essence, the flow between the axial stations defined by the FSP and the onset of reattachment appears to be a free turbulent jet that is mixing with a nearly one-dimensional outer flow. Of course, the velocity of this outer flow varies considerably in the axial direction.

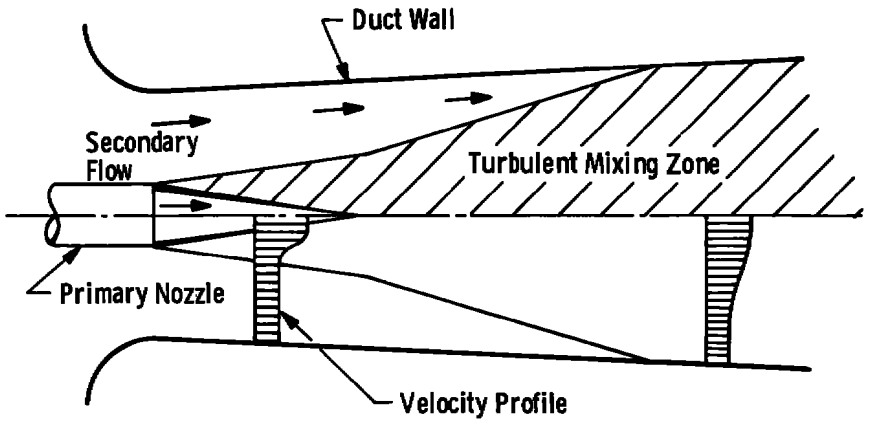

a. Flow without recirculation

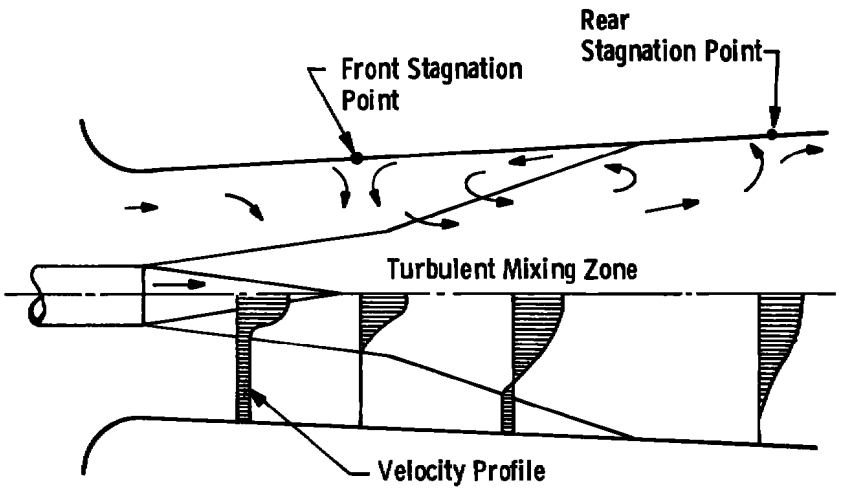

b. Flow with recirculation

Figure 1. Schematic of ducted mixing processes.

The wall boundary layers are very thin in the region of recirculating flow, and wall viscous effects seem to be important only far downstream of the RSP (Ref. 4).

Flows with recirculation are truly elliptic in nature because, in certain regions, the axial flow gradients become large compared with the lateral gradients. Therefore, an accurate analysis of recirculating flows must be based on solution of the Navier-Stokes

equations. During the past several years, much progress has been made on numerical techniques for solving these equations. For example, the finite-difference analysis of Gosman, et al. (Ref. 8), has been widely used for predicting recirculating flow fields. But in spite of the potential of the finite-difference approach, there are several reasons why this approach cannot yet be considered a reliable analytical tool for routine engineering applications (Refs. 9 and 10). First, with an adequately fine mesh for the flow configurations of interest, the computation time is large. Second, there are unresolved accuracy problems in the numerical algorithms; finite-difference solutions of combustor flows commonly do not conserve fuel species to an acceptable degree. Third, specification of boundary conditions is difficult and is often done in an arbitrary manner. Finally, as with any analysis of turbulent flow, an adequate semi-empirical model of the turbulent transport processes must be specified; with the finite-difference approach, the transport model must be applicable to every point in the flow field.

There is a simpler approach to the engineering computation of ducted flows with recirculation. The integral form of the boundary-layer equations can be used to describe flows with recirculation if the profile shapes for velocity, species, etc., are specified. Hill (Refs. 4 and 11) used this integral approach to predict constant-density ducted flows with recirculation. Of course, the streamwise turbulent transport terms are neglected in this approach, which results in a poor description of the flow in some regions. But the overall flow field predictions are adequate for many engineering purposes, and the integral method is computationally efficient. In addition, the very nature of the integral method ensures that momentum, species, etc., are conserved.

In this report, the integral approach is applied to the prediction of variable-density ducted turbulent flows with and without recirculation. Flows with equilibrium chemical reactions are included in the formulation. The flow geometry considered is either axisymmetric or planar, and provision is made to calculate flows with an arbitrary centerbody. In the "basic" integral analysis described in Section 2.0, the streamwise turbulent transport terms are neglected. The predictions of the basic analysis are compared with available experimental results in Section 3.0, and the regions of the flow that are poorly predicted are identified. An "extended" integral analysis, in which the streamwise turbulent transport terms are included, is described in Section 4.0.

2.0 FORMULATION OF BASIC INTEGRAL ANALYSIS

The mathematical approach used in the present analysis is similar to that used for the "1-D Core Theory" of Ref. 2. Indeed, the present analysis can be considered an extension and a refinement of the "1-D Core Theory," which is applicable only to axisymmetric flows without recirculation.

2.1 FLOW REGIMES

Several flow regimes[1] can occur in a ducted turbulent flow. These regimes are characterized by the width and position of the turbulent shear layer and by whether or not the flow recirculates. The integral analysis must be formulated differently for each of the flow regimes. The flow regimes that can occur in a nonrecirculating flow are illustrated in Fig. 2, and the regimes that can occur in a ducted flow with recirculation are illustrated in Fig. 3. Thus, there are six possible flow regimes and five possible sequences of these regimes.

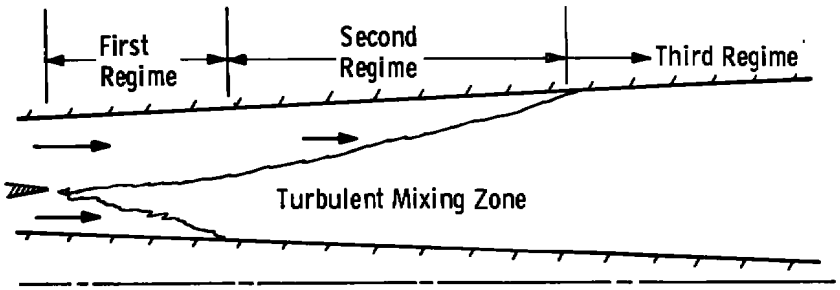

a. Mixing zone propagates to centerbody before it propagates to duct wall

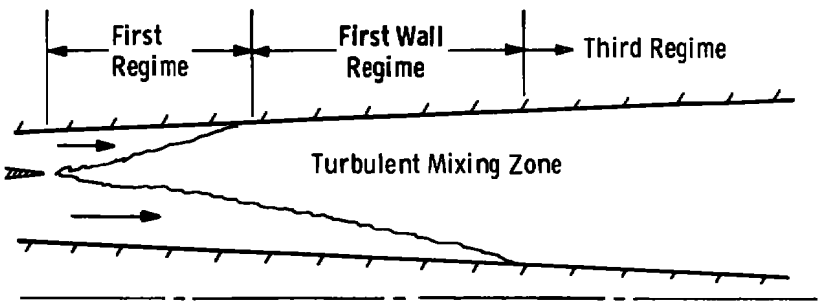

b. Mixing zone propagates to duct wall before it propagates to centerbody

Figure 2. Possible sequences of regimes for flow without recirculation.

[1] In the nomenclature used to describe the regimes, "first" indicates a regime in which there is a potential core of jet fluid between the centerbody and the inner edge of the shear layer. "Second" indicates a regime in which the shear layer extends to the centerbody but has not yet reached the duct wall. "Wake" indicates a regime in which a region of reversed flow exists between the outer edge of the shear layer and the duct wall.

Note that, when the initial value of the secondary velocity is zero, the "first" regime (Fig. 3) will not occur, and recirculation will begin at the duct entrance (in the "first wake" regime).

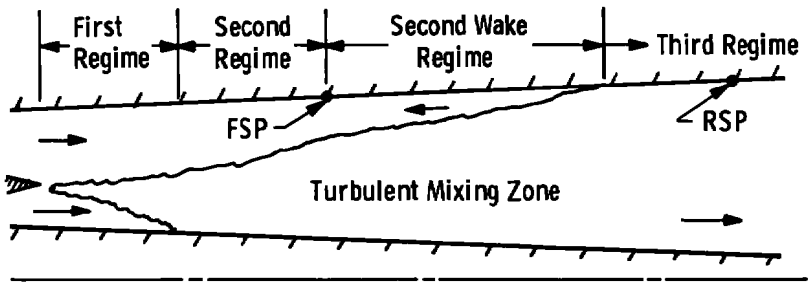

a. Recirculation begins in second regime

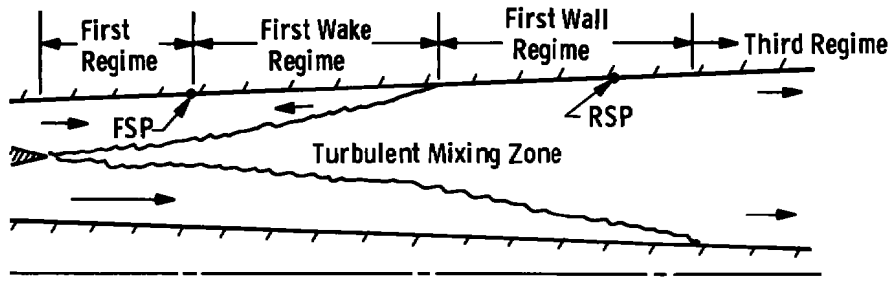

b. Recirculation begins in first regime and mixing zone propagates to duct wall before it propagates to centerbody

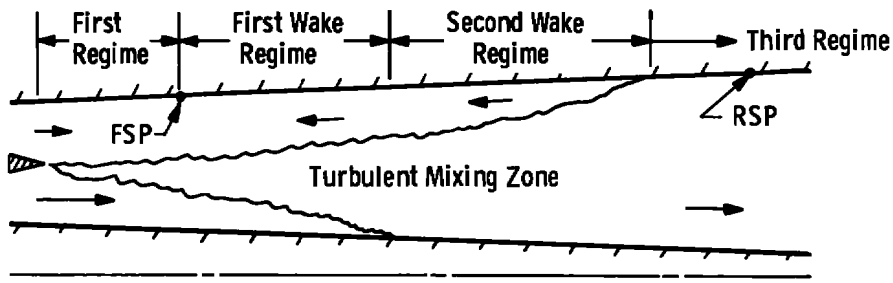

c. Recirculation begins in first regime and mixing zone propagates to centerbody before it propagates to duct wall

Figure 3. Possible sequences of regimes for flow with recirculation.

2.2 BASIC ASSUMPTIONS

The principal assumptions used in the analysis are:

1. The flow is steady and either planar or axisymmetric.

2. All gases obey the perfect gas law.

3. The flow is described by the integral form of the boundary-layer equations.

4. The turbulent Prandtl and Schmidt numbers are unity.

5. The mixing layer is fully turbulent (negligible laminar transport), and the initial boundary layers are negligible.

6. The mixing layer velocity profiles are shape-similar and are represented by a cosine function.

7. The inviscid portions of the primary and secondary flows are one-dimensional and isentropic (first, first wake, first wall, and second regimes).

8. For mixing with simultaneous chemical reactions, the reactions are in equilibrium.

9. The duct and centerbody surfaces are frictionless and adiabatic.

10. The static pressure is constant in the first wake and second wake regimes.

11. In the wake region, between the outer edge of the shear layer and the duct wall, the axial component of velocity and the element species are one-dimensional (first wake and second wake regimes).

2.3 BASIC EQUATIONS

The basic boundary-layer equations are:

Continuity

$$\frac{\partial}{\partial x}(\rho u r^{\alpha}) + \frac{\partial}{\partial r}(\rho v r^{\alpha}) = 0 \tag{1}$$

where

$\alpha = 0$ for planar flow

$\alpha = 1$ for axisymmetric flow

Axial Momentum

$$\rho u r^{\alpha} \frac{\partial u}{\partial x} + \rho v r^{\alpha} \frac{\partial u}{\partial r} = \frac{\partial}{\partial r}\left(\rho \epsilon r^{\alpha} \frac{\partial u}{\partial r}\right) - r^{\alpha} \frac{\partial p}{\partial x} \tag{2}$$

where ϵ is the turbulent eddy viscosity.

Energy

$$\rho u r^{\alpha} \frac{\partial H}{\partial x} + \rho v r^{\alpha} \frac{\partial H}{\partial r} = \frac{\partial}{\partial r}\left(\rho \epsilon r^{\alpha} \frac{\partial H}{\partial r}\right) \tag{3}$$

Element Species Conservation

$$\rho u r^{\alpha} \frac{\partial C_i}{\partial x} + \rho v r^{\alpha} \frac{\partial C_i}{\partial r} = \frac{\partial}{\partial r}\left(\rho \epsilon r^{\alpha} \frac{\partial C_i}{\partial r}\right) \tag{4}$$

Nomenclature for the integral analysis is shown in Figs. 4 and 5. Equations (1), (2), and (4) are integrated (Ref. 2) to obtain five integral equations: (1) a continuity equation for the entire flow, (2) a momentum equation for the entire flow, (3) a momentum equation for the flow between the centerbody surface (r_c) and r_m (where $r_m = r_i + b/2$), (4) a species conservation equation for the entire flow, and (5) a species conservation equation for the flow between r_c and r_m.

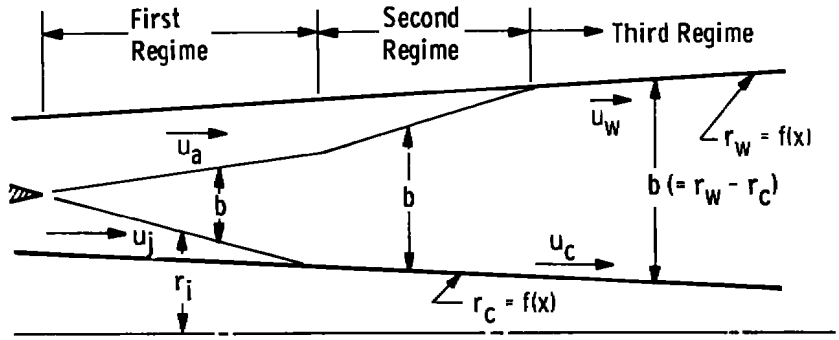

a. Mixing zone propagates to centerbody before it propagates to duct wall

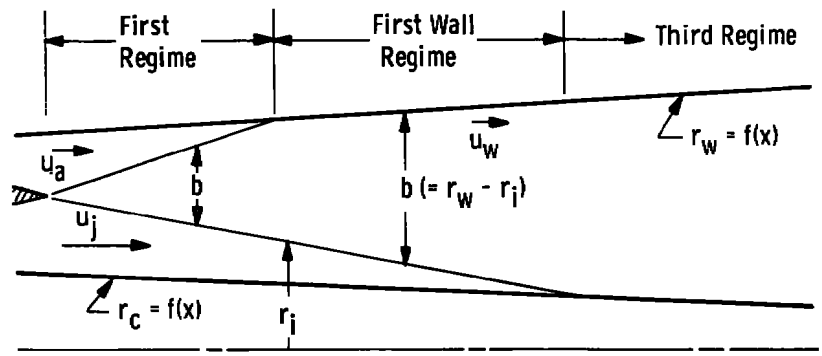

b. Mixing zone propagates to duct wall before it propagates to centerbody

Figure 4. Nomenclature for integral analysis of flow without recirculation.

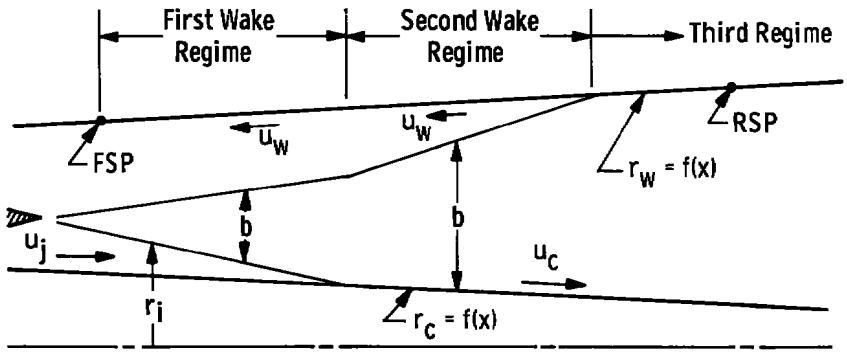

Figure 5. Nomenclature for integral analysis of flow with recirculation.

The integral equation are:

Overall Continuity

$$\int_{r_c}^{r_w} \frac{\partial}{\partial x} (\rho u)\, r^{\alpha}\, dr = \rho_c u_c r_c^{\alpha} \frac{dr_c}{dx} - \rho_w u_w r_w^{\alpha} \frac{dr_w}{dx} \tag{5}$$

where the subscript "c" indicates properties along the centerbody surface and the subscript "w" indicates properties along the duct wall.

Overall Momentum

$$\int_{r_c}^{r_w} \frac{\partial}{\partial x} (\rho u^2)\, r^{\alpha}\, dr = \rho_c u_c^2 r_c^{\alpha} \frac{dr_c}{dx} - \rho_w u_w^2 r_w^{\alpha} \frac{dr_w}{dx} - \frac{\left[r_w^{\alpha+1} - r_c^{\alpha+1}\right]}{(\alpha + 1)} \frac{dp}{dx} \tag{6}$$

Half-Radius Momentum

$$\int_{r_c}^{r_m} \frac{\partial}{\partial x} (\rho u^2)\, r^{\alpha}\, dr - u_m \int_{r_c}^{r_m} \frac{\partial}{\partial x} (\rho u)\, r^{\alpha}\, dr = \tau_m r_m^{\alpha} - (u_c - u_m) \rho_c u_c r_c^{\alpha} \frac{dr_c}{dx} - \frac{\left[r_m^{\alpha+1} - r_c^{\alpha+1}\right]}{(\alpha - 1)} \frac{dp}{dx} \tag{7}$$

where the subscript "m" indicates the properties along r_m and τ_m is a turbulent shear stress.

Overall Species

$$\int_{r_c}^{r_w} \frac{\partial}{\partial x} (\rho u C)\, r^{\alpha}\, dr = \rho_c u_c C_c r_c^{\alpha} \frac{dr_c}{dx} - \rho_w u_w C_w r_w^{\alpha} \frac{dr_w}{dx} \tag{8}$$

Half-Radius Species

$$\int_{r_c}^{r_m} \frac{\partial}{\partial x} (\rho u C)\, r^{\alpha}\, dr - C_m \int_{r_c}^{r_m} \frac{\partial}{\partial x} (\rho u)\, r^{\alpha}\, dr = q_m r_m^{\alpha} - \rho_c u_c (C_c - C_m) r_c^{\alpha} \frac{dr_c}{dx} \tag{9}$$

where q_m is a turbulent species flux.

Because the flow is one-dimensional for $r_c < r < r_i$ and for $(r_i + b) < r < r_w$, the integral equations can be rewritten as

Overall Continuity

$$\frac{\left[r_i^{\alpha+1} - r_c^{\alpha+1}\right]}{(\alpha+1)} \frac{d}{dx}(\rho_c u_c) + \int_{r_1}^{r_i - b} \frac{\partial}{\partial x}(\rho u) r^\alpha dr + \frac{\left[r_w^{\alpha+1} - (r_1 - b)^{\alpha-1}\right]}{(\alpha+1)} \frac{d}{dx}(\rho_w u_w)$$
$$= \rho_c u_c r_c^\alpha \frac{dr_c}{dx} - \rho_w u_w r_w^\alpha \frac{dr_w}{dx} \tag{10}$$

Overall Momentum

$$\frac{\left[r_i^{\alpha+1} - r_c^{\alpha-1}\right]}{(\alpha+1)} \frac{d}{dx}(\rho_c u_c^2) - \int_{r_1}^{r_i + b} \frac{\partial}{\partial x}(\rho u^2) r^\alpha dr + \frac{\left[r_w^{\alpha+1} - (r_i + b)^{\alpha+1}\right]}{(\alpha+1)} \frac{d}{dx}(\rho_w u_w^2)$$
$$= \rho_c u_c^2 r_c^\alpha \frac{dr_c}{dx} - \rho_w u_w^2 r_w^\alpha \frac{dr_w}{dx} - \frac{\left[r_w^{\alpha+1} - r_c^{\alpha+1}\right]}{(\alpha+1)} \frac{dp}{dx} \tag{11}$$

Half-Radius Momentum

$$\frac{\left[r_i^{\alpha+1} - r_c^{\alpha+1}\right]}{(\alpha+1)} \frac{d}{dx}(\rho_c u_c^2) + \int_{r_i}^{r_m} \frac{\partial}{\partial x}(\rho u^2) r^\alpha dr - u_m \frac{\left[r_i^{\alpha+1} - r_c^{\alpha+1}\right]}{(\alpha+1)} \frac{d}{dx}(\rho_c u_c)$$
$$- u_m \int_{r_i}^{r_m} \frac{\partial}{\partial x}(\rho u) r^\alpha dr = r_m r_m^\alpha + (u_c - u_m) \rho_c u_c r_c^\alpha \frac{dr_c}{dx} - \frac{\left[r_m^{\alpha+1} - r_c^{\alpha+1}\right]}{(\alpha+1)} \frac{dp}{dx} \tag{12}$$

Overall Species

$$\frac{\left[r_i^{\alpha+1} - r_c^{\alpha+1}\right]}{(\alpha+1)} \frac{d}{dx}(\rho_c u_c C_c) + \int_{r_1}^{r_i - b} \frac{\partial}{\partial x}(\rho u C) r^\alpha dr + \frac{\left[r_w^{\alpha+1} - (r_i + b)^{\alpha+1}\right]}{(\alpha+1)} \frac{d}{dx}(\rho_w u_w C_w)$$
$$= \rho_c u_c C_c r_c^\alpha \frac{dr_c}{dx} - \rho_w u_w C_w r_w^\alpha \frac{dr_w}{dx} \tag{13}$$

Half-Radius Species

$$\frac{\left[r_i^{\alpha+1} - r_c^{\alpha+1}\right]}{(\alpha+1)} \frac{d}{dx}(\rho_c u_c C_c) + \int_{r_i}^{r_m} \frac{\partial}{\partial x}(\rho u C) r^\alpha dr - C_m \frac{\left[r_i^{\alpha+1} - r_c^{\alpha+1}\right]}{(\alpha+1)} \frac{d}{dx}(\rho_c u_c)$$
$$- C_m \int_{r_1}^{r_m} \frac{\partial}{\partial x}(\rho u) r^\alpha dr = q_m r_m^\alpha - \rho_c u_c (C_c - C_m) r_c^\alpha \frac{dr_c}{dx} \tag{14}$$

Equations (10) through (14) apply to all six regimes shown in Figs. 2 and 3. Of course, r_1 goes to r_c in the second, second wake, and third regimes. In the first, first

wake, and first wall regimes, $C_c = C_j = 1$, and ρ_c and u_c are the isentropic variables (ρ_j and u_j). In the first and second regimes, $C_w = 0$, and ρ_w and u_w are the isentropic variables (ρ_a and u_a). The pressure gradient terms are zero in the first wake and second wake regimes.

2.4 SHEAR LAYER PROFILES

The shear layer velocity profile is described by

$$\frac{u - u_w}{u_c - u_w} = \frac{1}{2} - \frac{1}{2} \cos\left(\pi \frac{r - r_1}{b}\right) \tag{15}$$

The velocity at the half-radius control surface (r_m) is

$$u_m = \frac{1}{2}(u_c + u_w) \tag{16}$$

For a constant-pressure nonrecirculating flow, the element species concentration profile is related to the velocity profile by

$$\frac{C - C_w}{C_j - C_w} = \frac{u - u_w}{u_j - u_w} \tag{17}$$

Similarly, the total enthalpy profile is related to the velocity profile by

$$\frac{H - H_w}{H_j - H_w} = \frac{u - u_w}{u_j - u_w} \tag{18}$$

Thus, C, H, and u are linearly related in a constant-pressure nonrecirculating flow. This is the well-known Crocco integral solution obtained from Eqs. (2), (3), and (4). In the ducted mixing problem, however, the pressure gradient terms are negligible only in the first wake and second wake regimes. In addition, u_w, C_w, and H_w vary with x, even in the constant-pressure wake regimes. Therefore, Eqs. (17) and (18) cannot be used. The approach that has been taken in this study is to assume that the concentration-velocity relation can be expressed as

$$\frac{C - C_w}{C_j - C_w} = \left(\frac{u - u_w}{u_j - u_w}\right)^K \tag{19}$$

where K can be a function of x. The mixing zone concentration profiles described by Eqs. (15) and (19) are shown in Fig. 6 for various values of K. Note that a power-law relation similar to Eq. (19) has been used to describe profiles that deviate from the Crocco relation because of nonunity transport coefficient ratios in free turbulent flows

(Ref. 12). Also note that the linear relationship between H and C is retained, even for flows with recirculation.

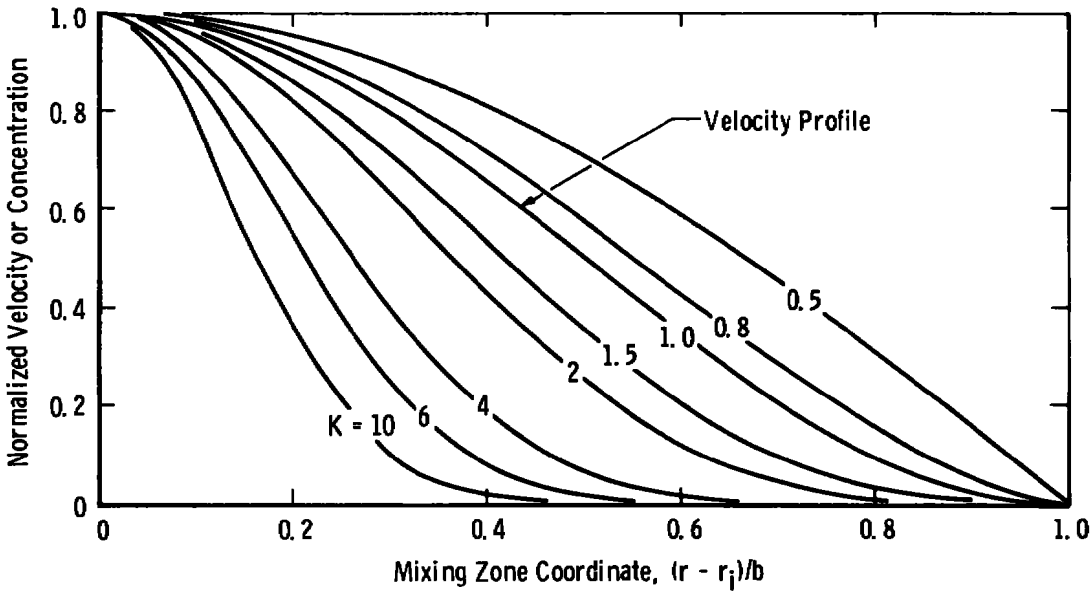

Figure 6. Mixing zone concentration and velocity profiles.

2.5 COMPUTATION OF DENSITY

For unity Prandtl and Schmidt numbers, the stagnation enthalpy and the gas properties are uniquely related to C, and the density field is calculated with the techniques described in Ref. 2. Namely, the stagnation temperature, specific heat, and gas constant are specified as a function of C, which varies from zero (pure outer stream gas) to one (pure jet gas). For chemically frozen flows, only the T_o, c_p, and R values at C = 0 and C = 1 need be specified. For flow with chemical reactions, an equilibrium chemistry analysis is used to specify T_o, c_p, and R as tabular functions of C.

At any point in the shear layer, u is given by Eq. (15), C is given by Eq. (19), and T_o, c_p, and R are determined. The density can then be obtained from the energy equation and the perfect gas law. Therefore, the density can be expressed functionally as

$$\rho = \rho(u, C, p) \tag{20}$$

2.6 TURBULENT TRANSPORT TERMS

The turbulent shear stress (τ_m) that appears in Eq. (12) is given by

$$\tau_m = \rho_m \epsilon \left.\frac{\partial u}{\partial r}\right|_m \tag{21}$$

where ϵ is the turbulent eddy viscosity. The turbulent species flux (q_m) that appears in Eq. (14) is given by

$$q_m = \rho_m \epsilon \left.\frac{\partial C}{\partial r}\right|_m \tag{22}$$

The eddy viscosity model used in this study is the same as that described in Ref. 2. Namely, the Prandtl model for free-turbulent flows is used, with the coefficient (k) taken to be a function of the half-radius Mach number (M_m).

Thus,

$$\epsilon = k\, b \left| u_c - u_w \right| \tag{23}$$

and

$$k = k_o \left[0.66 + 0.34 \exp\left(-3.42\, M_m^2\right)\right] \tag{24}$$

In the first and first wake regimes, k_o is set equal to 0.007. In the other four regimes, k_o is set equal to 0.011.

For nonrecirculating flows, this eddy viscosity model has been shown to provide reasonably accurate predictions as long as the secondary velocity (u_{a1}) is not larger than about 0.3 times the jet velocity (u_{j1}) (Ref. 2).

For flows with recirculation, the eddy viscosity model is modified somewhat. The predictions of the reattachment region (in the third or first wall regimes) are improved if the eddy viscosity is held constant, or "frozen," at the value that is computed at the beginning of reattachment. This modification is discussed further in Section 3.1.

2.7 METHOD OF SOLUTION

Sufficient information is available to transform Eqs. (10) through (14) into a system of ordinary differential equations that is linear in the derivatives of the dependent variables. The transformation procedure is described in Refs. 2 and 13.

First Regime - The flow is completely described by four parameters (p, r_i, b, K), so Eq. (14) is not used. The resulting system of equations is

$$N_1 \frac{dp}{dx} - N_2 \frac{dr_i}{dx} + N_3 \frac{db}{dx} + N_4 \frac{dK}{dx} = N_5 \tag{25}$$

where N ≡ F for the continuity equation, N ≡ G for the overall momentum equation, N ≡ H for the half-radius momentum equation, and N ≡ I for the overall species equation. The equations of the coefficients for all regimes are presented in Appendix A. The numerous auxiliary equations necessary for computation of the coefficients are developed in the same manner as described in Ref. 2.

After the coefficients are evaluated numerically, Eq. (25) is solved for the derivatives (dp/dx, dr_i/dx, db/dx, dK/dx) by use of a matrix factorization technique. The resulting equations for the derivatives are numerically integrated with a modified Euler technique (variable step size).

Second Regime - As in the first regime, the flow is fully described by four parameters; these are chosen to be (p. u_c, b, K) and the resulting system of equations is:

$$N_1 \frac{dp}{dx} + N_2 \frac{du_c}{dx} + N_3 \frac{db}{dx} - N_4 \frac{dK}{dx} = N_5 \tag{26}$$

Third Regime - The flow is fully described by five variables (u_w, u_c, p, C_w, K), and Eq. (14) is required. The resulting system of equations is

$$N_1 \frac{du_w}{dx} + N_2 \frac{du_c}{dx} + N_3 \frac{dp}{dx} + N_4 \frac{dC_w}{dx} + N_5 \frac{dK}{dx} = N_6 \tag{27}$$

where N ≡ J for the half-radius species equation.

First Wake Regime - The five dependent variables are (u_w, r_i, b, C_w, K), and the resulting system of equations is

$$N_1 \frac{du_w}{dx} + N_2 \frac{dr_i}{dx} + N_3 \frac{db}{dx} + N_4 \frac{dC_w}{dx} + N_5 \frac{dK}{dx} = N_6 \tag{28}$$

Second Wake Regime - The five dependent variables are (u_w, u_c, b, C_w, K), and the resulting system of equations is

$$N_1 \frac{du_w}{dx} + N_2 \frac{du_c}{dx} + N_3 \frac{db}{dx} + N_4 \frac{dC_w}{dx} + N_5 \frac{dK}{dx} = N_6 \tag{29}$$

First Wall Regime - The five dependent variables are (u_w, r_i, p, C_w, K), and the resulting system of equations is

$$N_1 \frac{du_w}{dx} + N_2 \frac{dr_i}{dx} + N_3 \frac{dp}{dx} + N_4 \frac{dC_w}{dx} + N_5 \frac{dK}{dx} = N_6 \tag{30}$$

Notes on the Computer Program - Which of the six regimes will occur in a given flow, and the sequence of these regimes, is generally not known beforehand. Therefore, a series of tests is incorporated in the computer program to automatically provide the correct sequence of regimes.

In the present computer program, the duct wall and centerbody geometries are each described by a pair of functions: a fourth-order polynomial in x describes the radius up to a prescribed axial station, after which the geometry is conical.

The basic integral analysis has been programmed for numerical solution with an IBM 370/165 digital computer. A typical flow field computation requires a CPU time of about 30 sec.

3.0 RESULTS AND DISCUSSION OF BASIC INTEGRAL ANALYSIS

For ducted flows without recirculation, the present analysis yields predictions that are nearly identical to those of the "1-D Core Theory" of Ref. 2. Therefore, the major emphasis in this section will be placed on comparing the predictions with experimental results for flows with imbedded recirculation regions.

Similarity parameters have been proposed to correlate the occurrence and extent of recirculation in constant-density axisymmetric flow (Refs. 14, 15, and 16). These similarity parameters are applicable to constant-area ducts without centerbodies. Perhaps the most widely used similarity parameter is that proposed by Becker, et al. (Ref. 16), which is commonly called the Curtet number:

$$C_t = u_k \Big/ \left[\left(u_{j1}^2 - u_{a1}^2 \right) \left(\frac{r_n}{r_w} \right)^2 + \frac{1}{2} u_{a1}^2 - \frac{1}{2} u_k^2 \right]^{1/2} \tag{31}$$

where r_n is the primary nozzle radius and

$$u_k = (u_{j1} - u_{a1}) \left(\frac{r_n}{r_w} \right)^2 + u_{a1} \tag{31a}$$

The relationship among C_t, u_{a1}/u_{j1}, and r_n/r_w is shown in Fig. 7.

Correlations of experimental data have shown that recirculation will occur when C_t is less than 0.7 to 0.9. In addition, experimental data on the axial location and extent of the recirculation region in various duct geometries are well correlated when plotted versus C_t.

Note that the Curtet number is not applicable to variable-density flows or to flows in ducts with variable cross-sectional area. Schulz (Ref. 9 and 17) derived a variable-density similarity parameter but found that it does not adequately correlate the location and extent of recirculation observed in variable-density experiments. That is, the variable-density results do not collapse onto the constant-density results when plotted versus the similarity parameter.

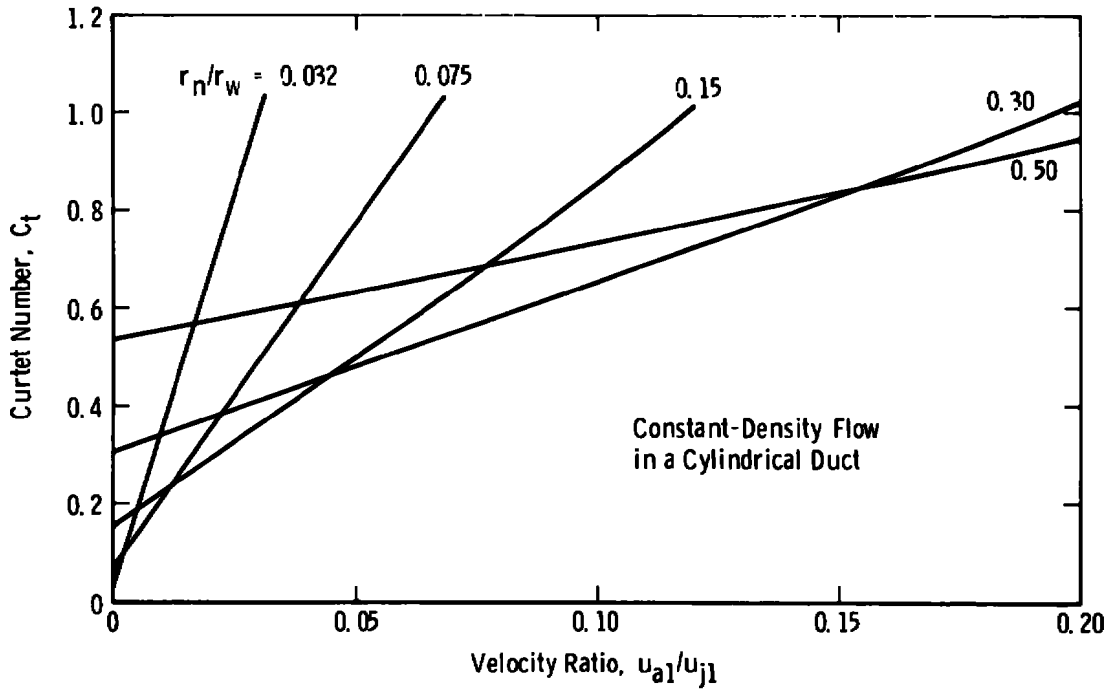

Figure 7. Curtet number as a function of velocity ratio.

3.1 EXPERIMENTS OF BARCHILON AND CURTET

Barchilon and Curtet (Ref. 7) conducted an extensive series of experiments on constant-density flows in a cylindrical duct. The nozzle-duct radius ratio (r_n/r_w) was 0.075, and the secondary-to-primary velocity ratio (u_{a1}/u_{j1}) was varied from zero to a value high enough to prevent recirculation. Predicted and experimental results for all six of the Barchilon and Curtet flows are shown in Figs. 8 through 10. Only Test No. 1 (C_t = 0.976) was conducted with a secondary velocity high enough to avoid recirculation along the duct wall.

Unless otherwise indicated on the figures, all the computations were made with the eddy viscosity "frozen" in the reattachment region (Section 2.6). Two of the flows, Tests

No. 4 and 6, were computed with both the frozen eddy viscosity model and the local eddy viscosity given by Eq. (23). The predicted distributions of wall velocity (Figs. 8d and f) show that the position of the RSP is predicted much better with the frozen viscosity. The need to arbitrarily freeze the eddy viscosity in the reattachment region is a

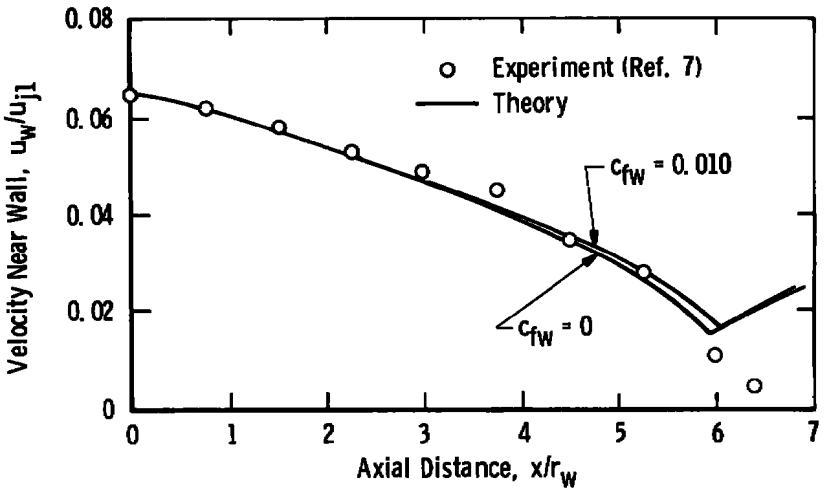

a. Test Number 1, C_t = 0.976, u_{a1}/u_{j1} = 0.0648

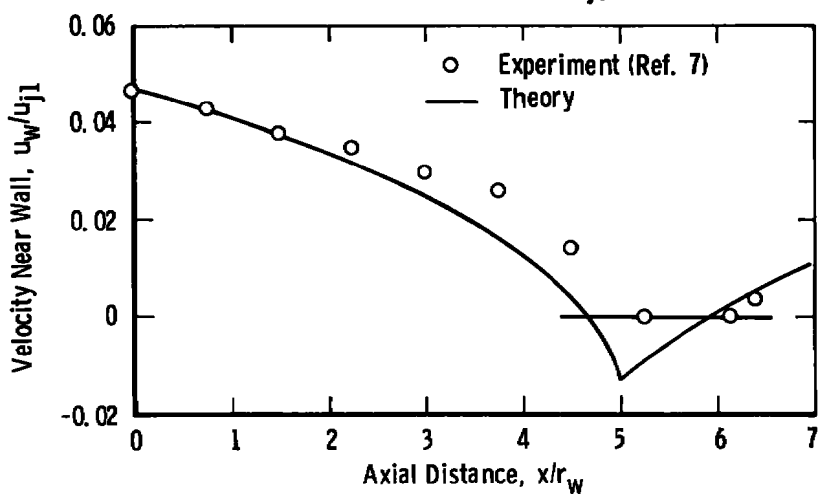

b. Test Number 2, C_t = 0.714, u_{a1}/u_{j1} = 0.0465

Figure 8. Wall velocity distributions for Barchilon and Curtet experiments.

result of the very strong history effects on the turbulence when the mean flow changes rapidly with distance. Simple local eddy viscosity models are clearly inadequate for rapidly changing flows such as occur in the reattachment region.

The predicted distributions of wall velocity (Figs. 8a through f) illustrate a characteristic feature of the integral solution. The magnitude of the peak reverse flow velocity is overpredicted, and a cusp is formed in the velocity distribution at the beginning of reattachment. In the region near the mixing zone attachment point,

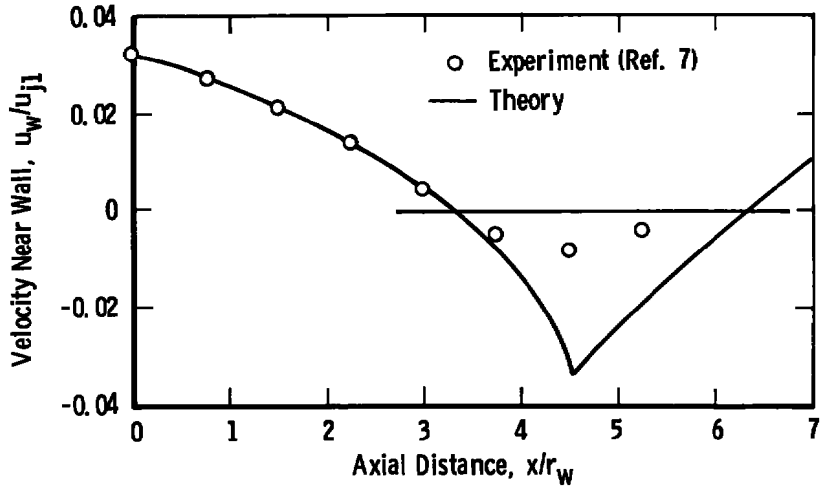

c. Test Number 3, C_t = 0.506, u_{a1}/u_{j1} = 0.0316

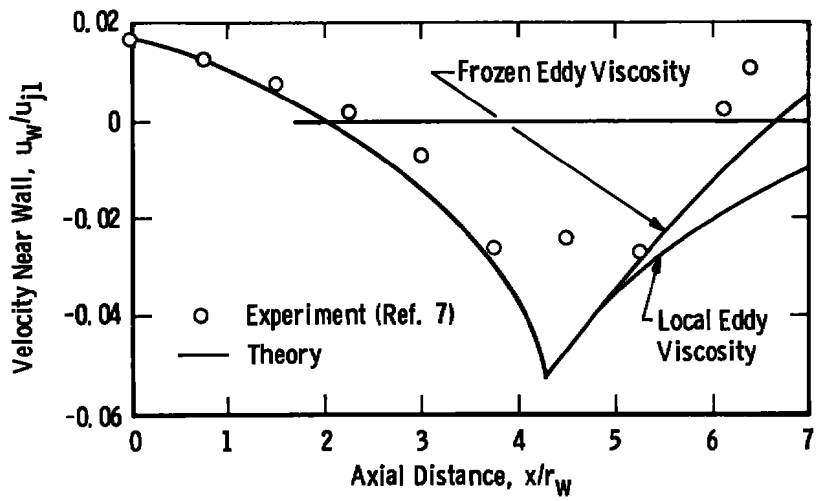

d. Test Number 4, C_t = 0.305, u_{a1}/u_{j1} = 0.0170

Figure 8. Continued.

streamwise turbulent transport of momentum is very significant. Of course, this streamwise momentum transport, which is neglected in the basic integral analysis, tends to round the cusp in the wall velocity distribution.

In spite of the locally unrealistic behavior of the predicted wall velocity distribution near the onset of reattachment, the solution seems to recover, and the slope of the velocity distribution at the RSP is fairly well predicted.

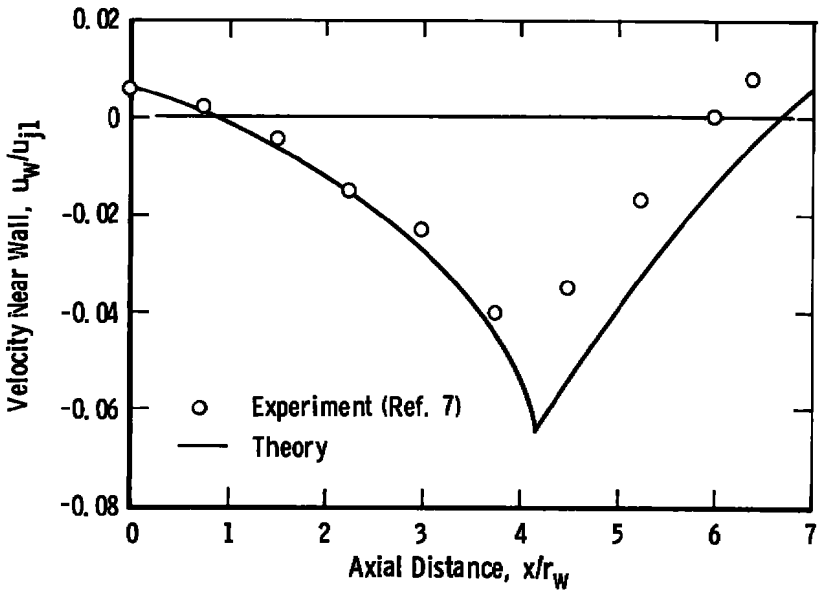

e. Test Number 5, $C_t = 0.152$, $u_{a1}/u_{j1} = 0.0057$

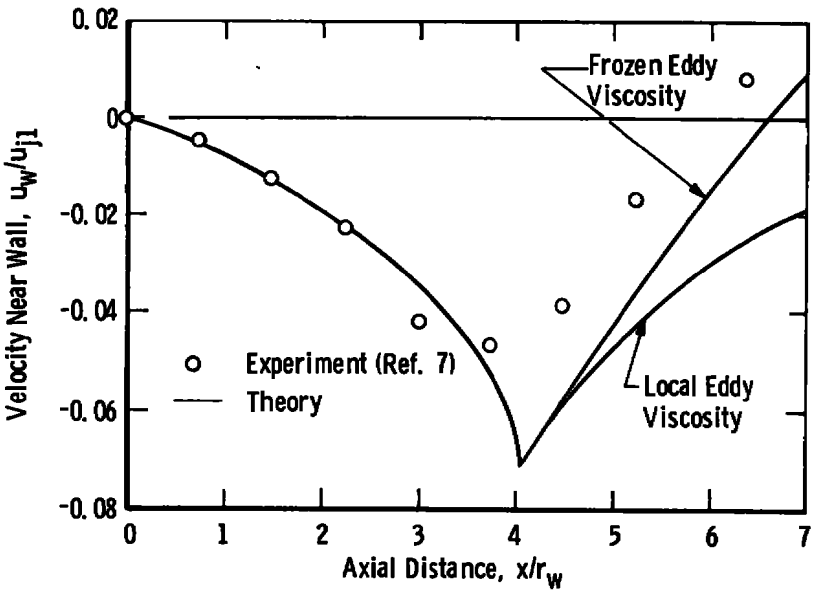

f. Test Number 6, $C_t = 0.075$, $u_{a1}/u_{j1} = 0$

Figure 8. Concluded.

Axial distributions of centerline velocity for the six Barchilon and Curtet flows are shown in Figs. 9a through f. In general, the predicted distributions are satisfactory.

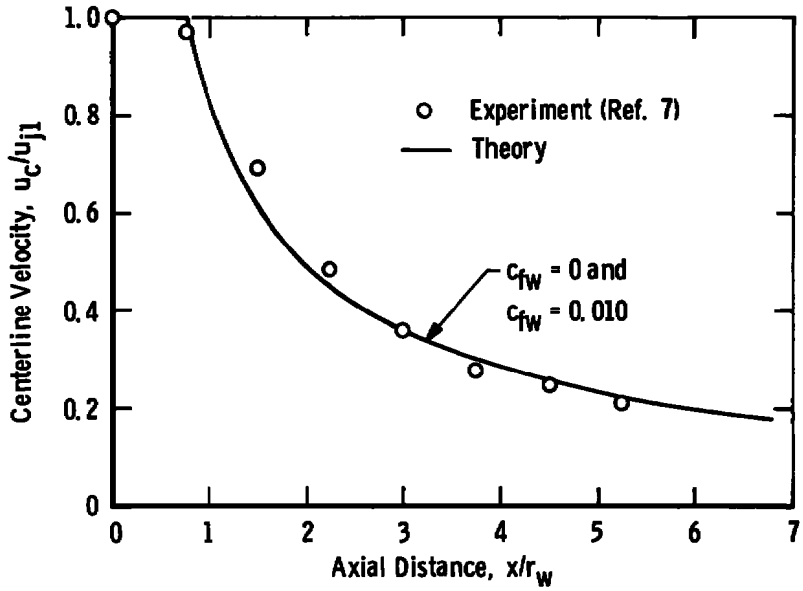

a. Test Number 1, C_t = 0.976, u_{a1}/u_{j1} = 0.0648

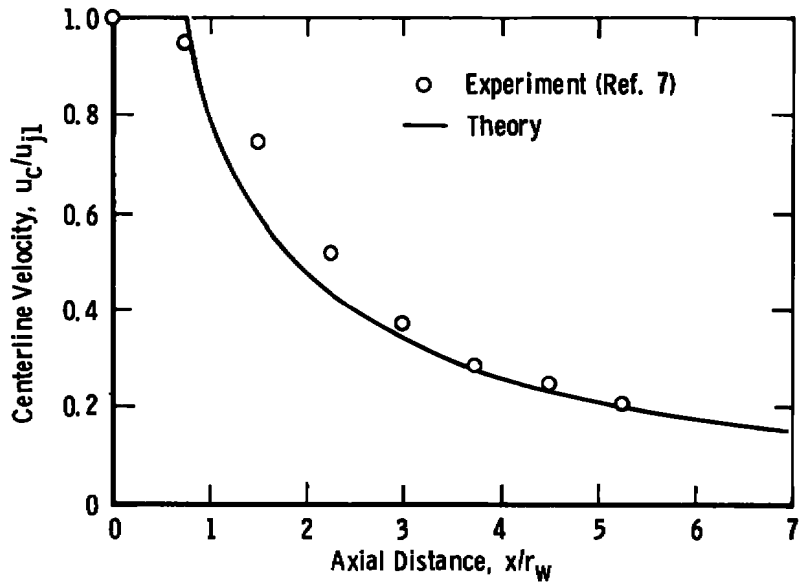

b. Test Number 2, C_t = 0.714, u_{a1}/u_{j1} = 0.0465

Figure 9. Centerline velocity distributions for Barchilon and Curtet experiments.

Figures 9d and f illustrate that the frozen eddy viscosity model yields slightly better predictions of the centerline velocity decay rate than does the local viscosity model.

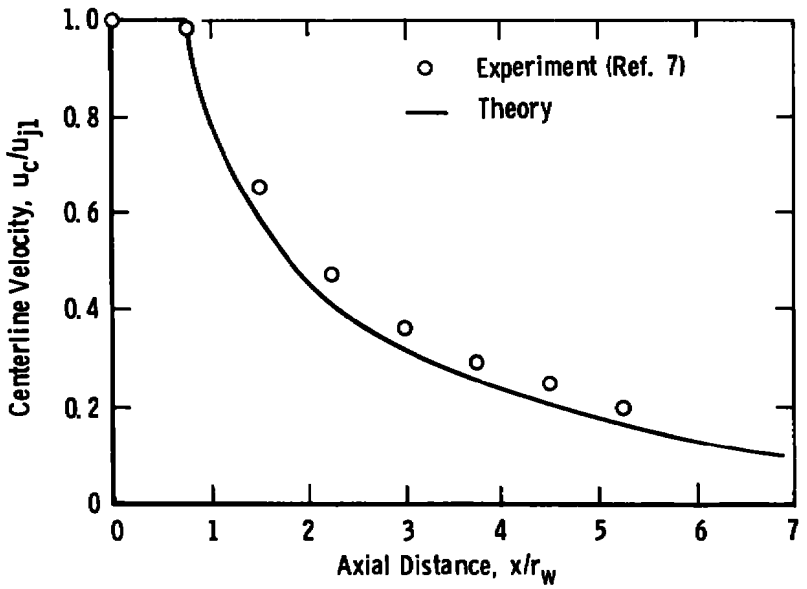

c. Test Number 3, C_t = 0.506, u_{a1}/u_{j1} = 0.0316

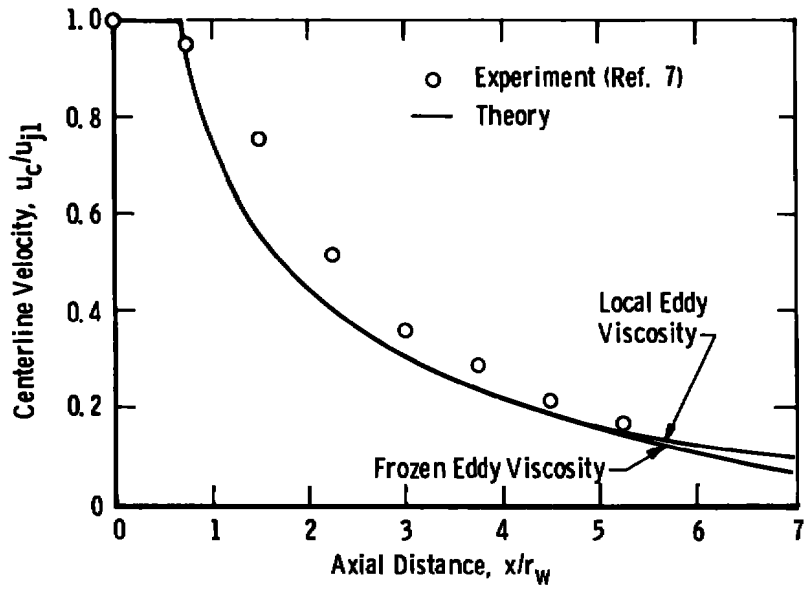

d. Test Number 4, C_t = 0.305, u_{a1}/u_{j1} = 0.0170

Figure 9. Continued.

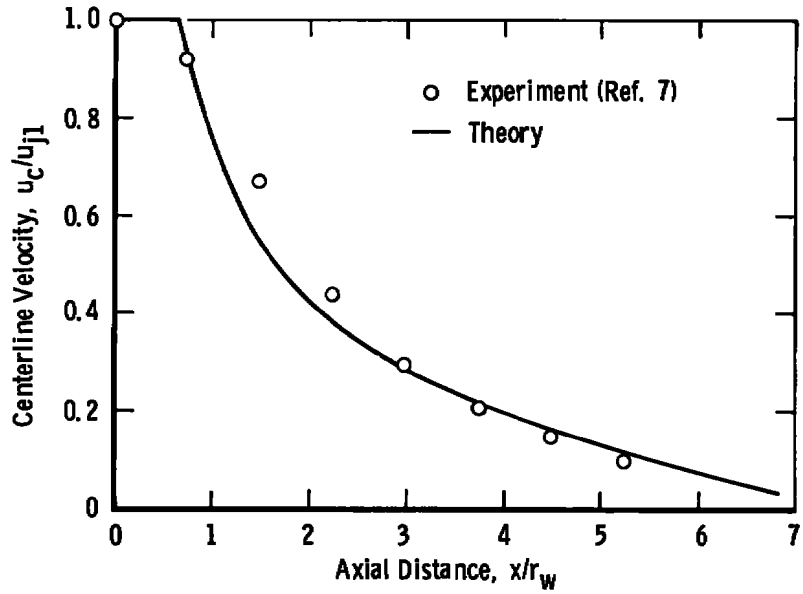

e. Test Number 5, C_t = 0.152, u_{s1}/u_{j1} = 0.0057

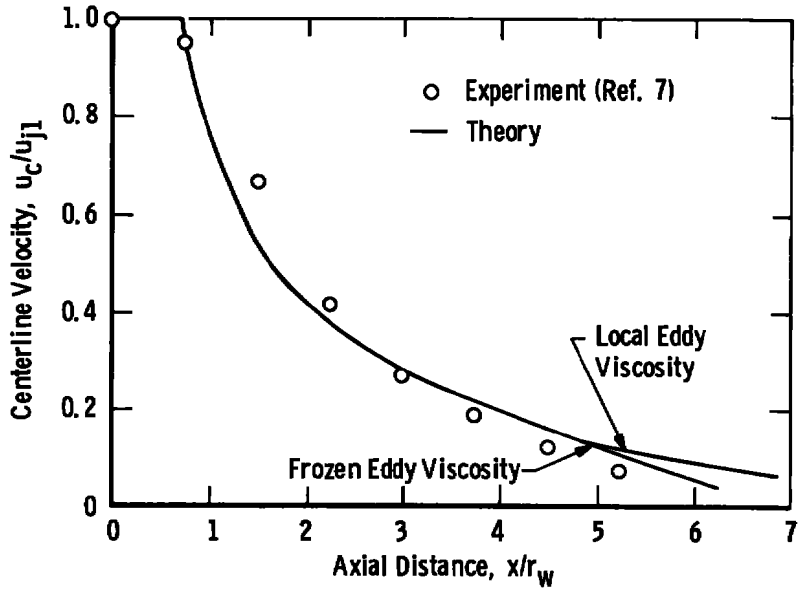

f. Test Number 6, C_t = 0.075, u_{s1}/u_{j1} = 0

Figure 9. Concluded.

Axial distributions of wall static pressure for the six flows are shown in Figs. 10a through f. In general, the predicted wall pressure in the reattachment region tends to rise too abruptly, and the peak wall pressure is overpredicted; this overprediction becomes larger as C_t is increased.

The static pressure in the first wake and second wake regimes is assumed to be constant. However, as shown in Figs. 10c through f, the experimental wall static pressures

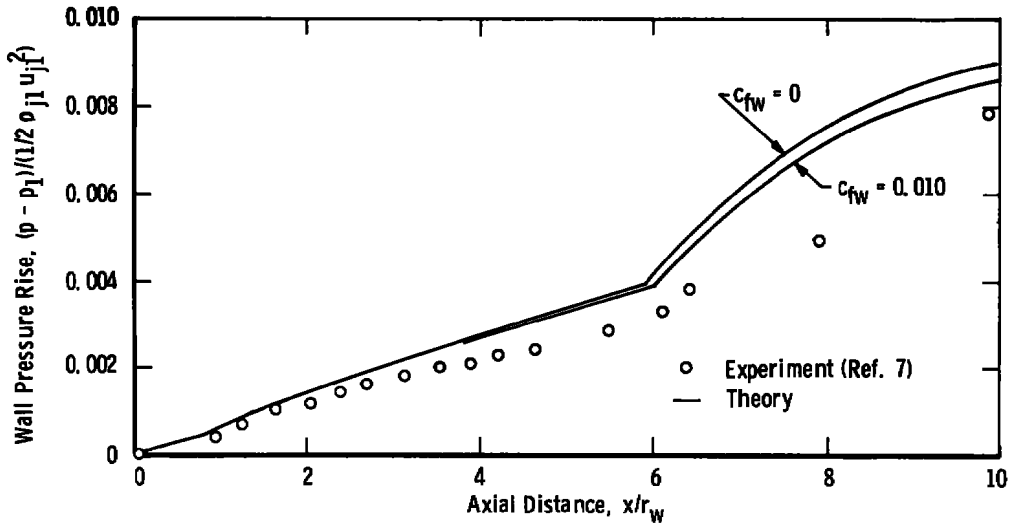

a. Test Number 1, $C_t = 0.976$, $u_{a1}/u_{j1} = 0.0648$

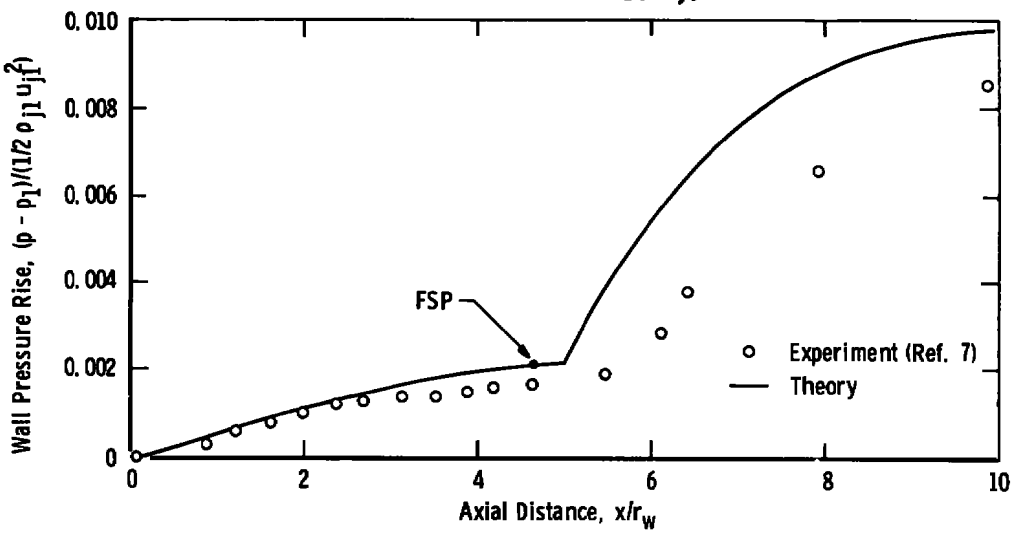

b. Test Number 2, $C_t = 0.714$, $u_{a1}/u_{j1} = 0.0465$

Figure 10. Wall pressure distributions for Barchilon and Curtet experiments.

decrease slightly with distance downstream of the FSP, until a minimum is reached at a station upstream of the predicted shear layer attachment point.

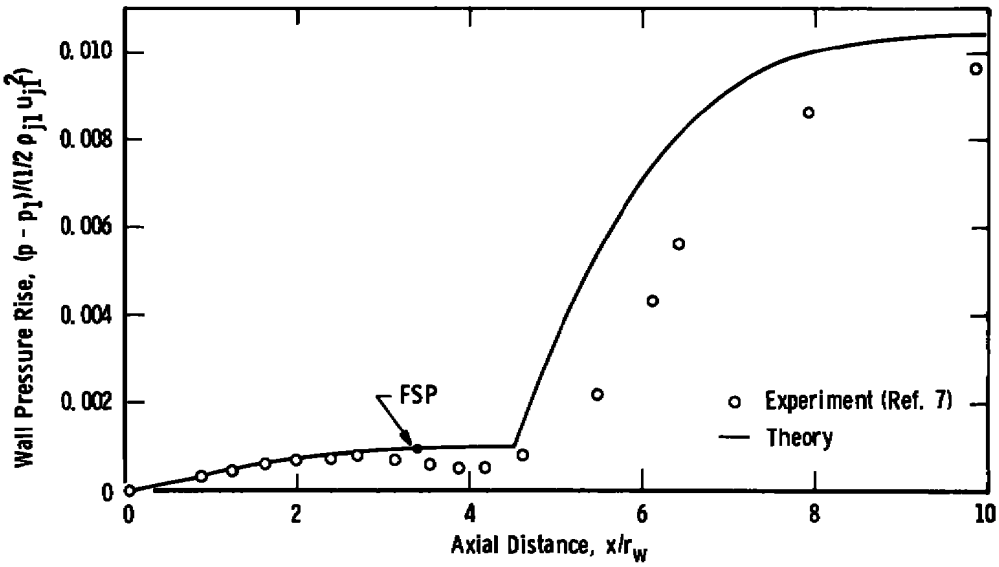

c. Test Number 3, $C_t = 0.506$, $u_{a1}/u_{j1} = 0.0316$

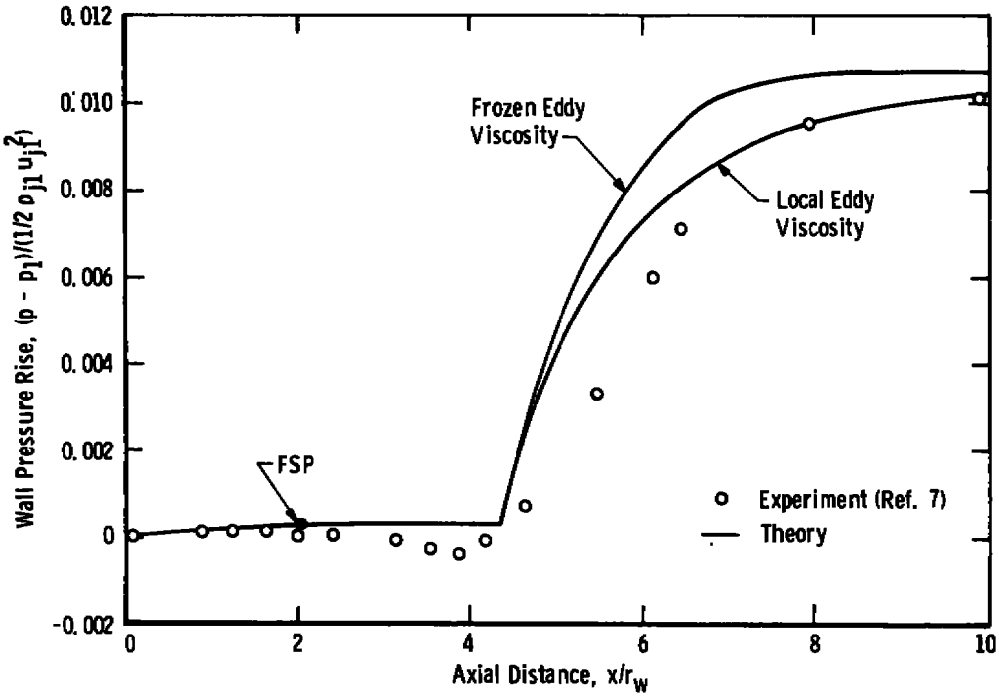

d. Test Number 4, $C_t = 0.305$, $u_{a1}/u_{j1} = 0.0170$

Figure 10. Continued.

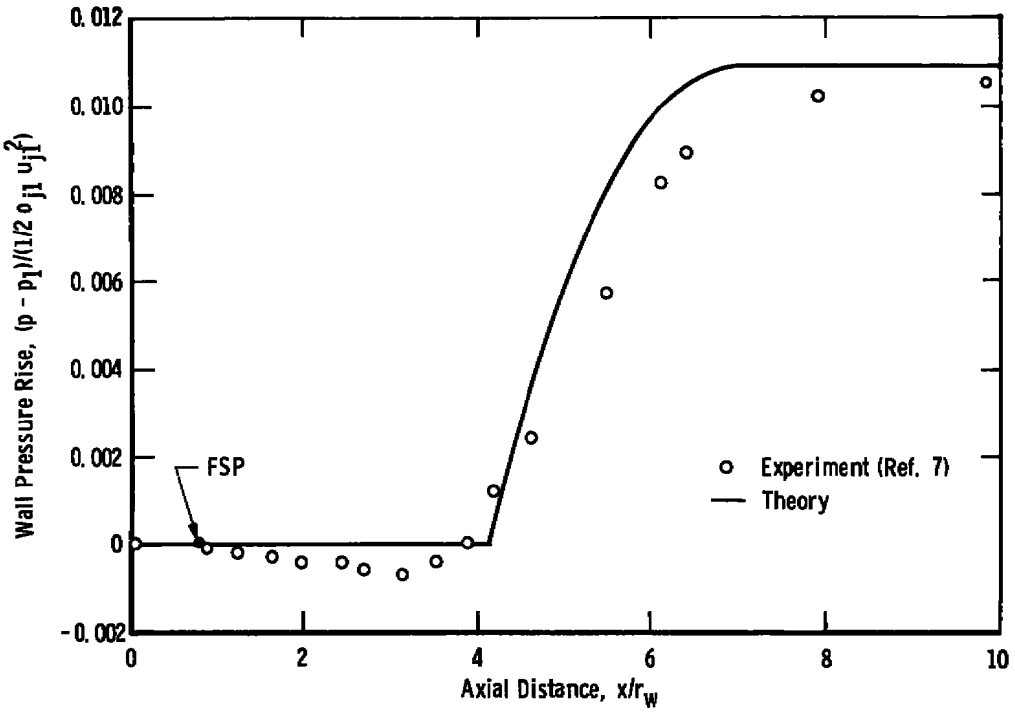

e. Test Number 5, $C_t = 0.152$, $u_{a1}/u_{j1} = 0.0057$

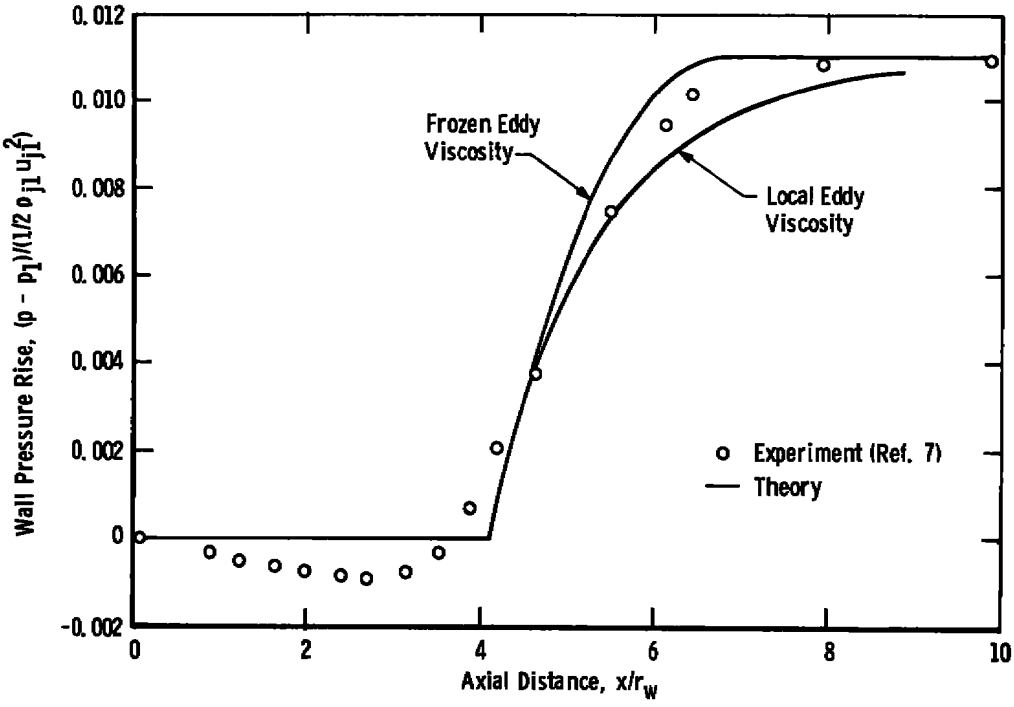

f. Test Number 6, $C_t = 0.075$, $u_{a1}/u_{j1} = 0$

Figure 10. Concluded.

In the integral analysis, the wall frictional effects are assumed to be negligible. To evaluate the validity of this assumption, a wall shear stress term was added to the right hand-side of Eq. (11); the shear stress is equal to $1/2\ c_{fw}\rho_w u_w^2$ where c_{fw} is the skin friction coefficient. As shown in Fig. 10a for $C_t = 0.976$, the effect of even a fairly large value of c_{fw} on the pressure distribution is small. And the effect on the u_w and u_c distributions is negligible (Figs. 8a and 9a). For flows with recirculation, the effect of wall friction is even smaller than that shown for $C_t = 0.976$.

Distances from the entrance of the mixing duct to the front and rear stagnation points are shown in Fig. 11 for the Barchilon and Curtet flows. The analysis predicts no recirculation for C_t greater than 0.84; on the other hand, the experiments show that recirculation persists for C_t values up to about 0.95. The predicted effect of the secondary-primary velocity ratio on the location of the FSP is in excellent agreement with the experimental results. These experiments show that the location of the RSP is independent of C_t; the analysis predicts that the distance to the RSP is a mild function of C_t.

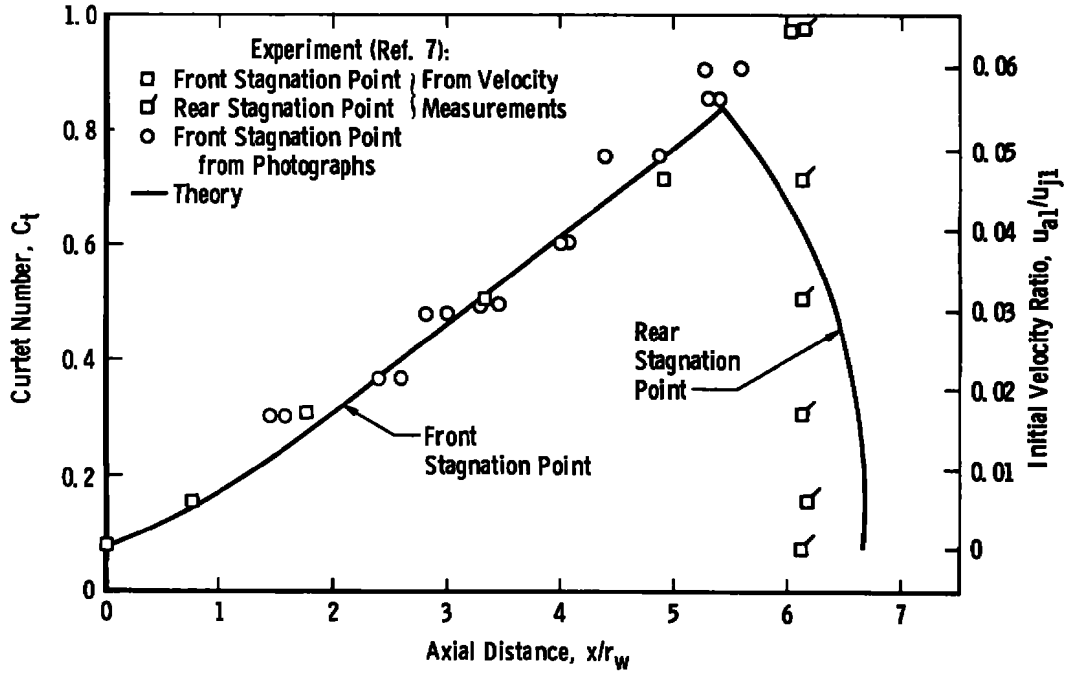

Figure 11. Extent of recirculation zone for Barchilon and Curtet experiments.

The analysis yields complete spatial distributions of the axial velocity component (u) and the density (ρ) in the flow field. By integrating the continuity equation between the axis and a particular streamline, the geometry of that streamline can be determined. These computations were carried out for several streamlines in the recirculation region of the Barchilon and Curtet Test No. 6 flow. As shown in Fig. 12, the predicted streamline shapes are realistic; in addition, they are in fairly good agreement with the experimental shapes (Ref. 7). The largest differences between the predicted and experimental streamline shapes occur near the duct entrance, for x/r_w less than one; these differences are attributed to deviations from one-dimensionality in the experimental wake region u profiles.

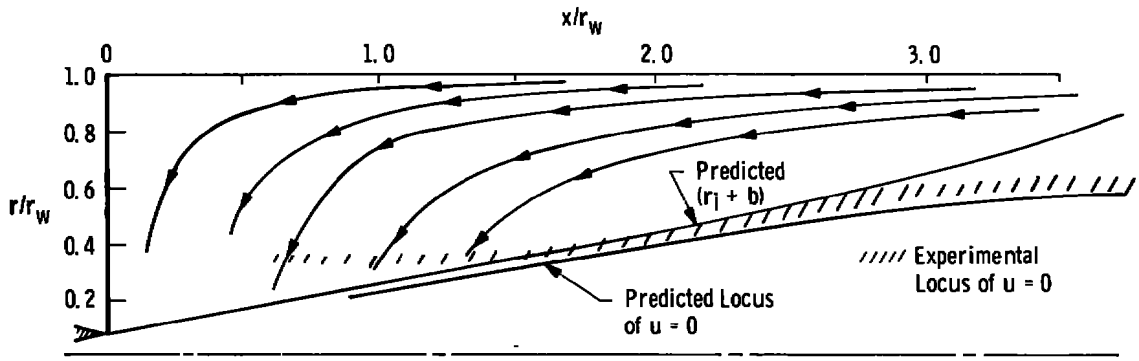

Figure 12. Predicted streamline pattern for Barchilon and Curtet Test No. 6 ($u_{a1}/u_{j1} = 0$).

Predicted and experimental loci of u = 0 are also shown in Fig. 12. The predicted locus is satisfactory for x/r_w greater than one, but is less so near the duct entrance.

3.2 EXPERIMENT OF HESKESTAD

In the Barchilon and Curtet recirculating flow experiments, r_n/r_w was only 0.075, and the turbulent mixing layer reached the axis well upstream of its intersection with the duct wall. Therefore, the flow pattern was as shown in Fig. 3a or Fig. 3c, and the entire reattachment process occurred in the third regime. For much larger values of r_n/r_w, say 0.5, the shear layer will reach the duct wall before it reaches the axis, and the flow pattern shown in Fig. 3b will be observed.

Heskestad (Ref. 18) measured the wall pressure distribution in a constant-density axisymmetric sudden-expansion flow; u_{ai}/u_{ji} was zero and r_n/r_w was 0.498. The predicted pressure distribution, obtained with the eddy viscosity frozen in the

reattachment region, is in good agreement with the experimental distribution (Fig. 13). As shown in the figure, reattachment begins in the first wall regime; however, the predicted RSP occurs just downstream of the transition to the third regime.

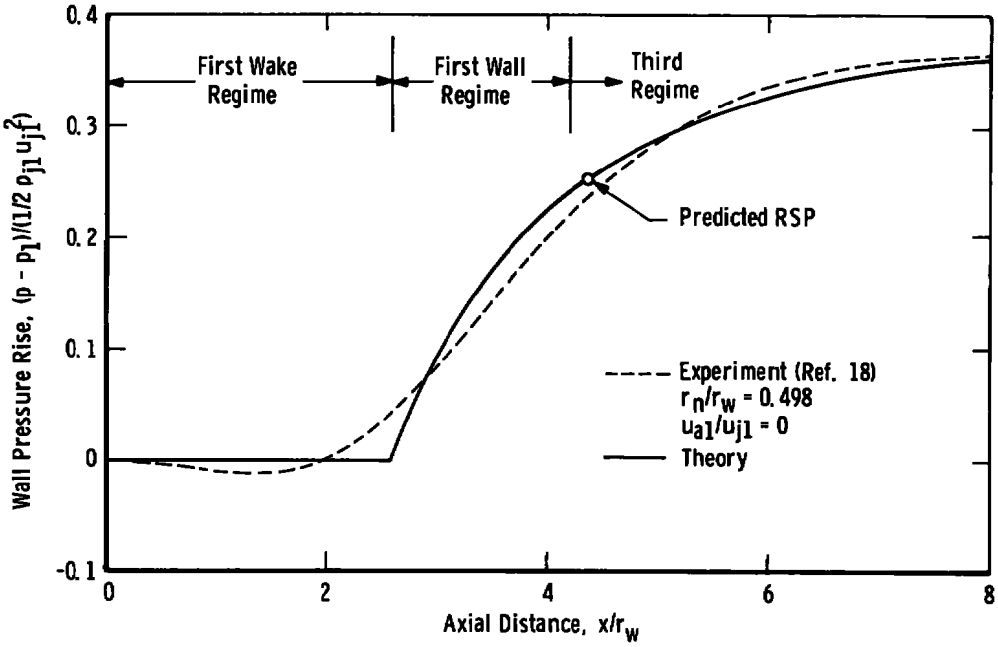

Figure 13. Wall pressure distribution for the experiment of Heskestad.

The predicted results obtained for the Heskestad geometry, as well as those obtained for the Barchilon and Curtet geometry, indicate that the concept of freezing the eddy viscosity in the reattachment region is successful for a variety of configurations. Therefore, all of the calculations described in the remainder of this report were obtained with the frozen viscosity model.

3.3 EXPERIMENTS OF BECKER, ET AL.

Becker, Hottel, and Williams (Refs. 16 and 19) conducted a series of experiments on constant-density axisymmetric flow with recirculation. The nozzle-duct radius ratio (r_n/r_w) was 0.032. Therefore, reattachment occurred in the third regime. In addition to measuring the mean velocity field in their experiments, Becker, et al., measured optically the concentration field by use of a smoke tracer in the jet.

The axial location and extent of recirculation measured by Becker, et al., is shown in Fig. 14, along with the predictions of the integral theory. Also shown in the figure are the predictions for the geometry of Barchilon and Curtet; the predictions for the two

geometries differ little when plotted as a function of C_t. In contrast to the Barchilon and Curtet results on the location of the RSP (Fig. 11), the results of Becker, et al., substantiate the predicted trend that the location of the RSP depends somewhat on the Curtet number.

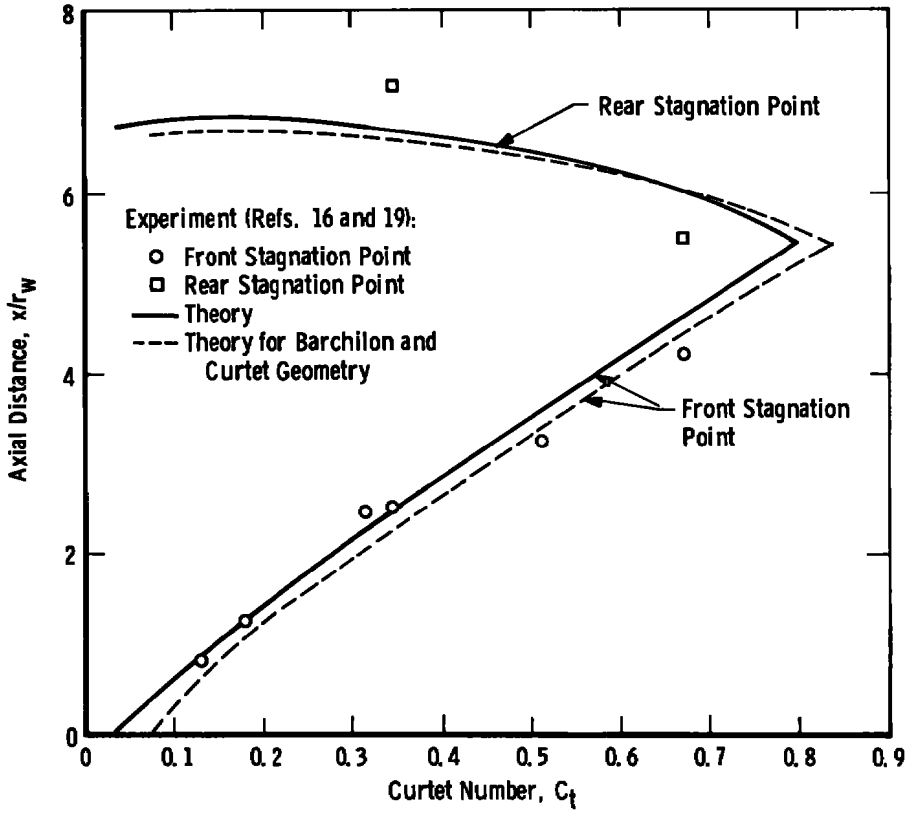

Figure 14. Axial extent of recirculation for the experiments of Becker, et al.

Axial distributions of jet species concentration at the duct wall (C_w) are shown in Fig. 15 for the three values of C_t investigated by Becker, et al. The predicted locations of the FSP's are indicated by arrows on the abscissa; as shown in Fig. 14, these predicted FSP locations are in excellent agreement with the experimental locations. The experimental C_w values become significant at an axial station about one duct radius upstream of the corresponding FSP. Indeed, the experimental distribution for $C_t = 0.137$ indicates that pure secondary-stream fluid exists nowhere in the flow field, even at $x = 0$.

The predicted C_w distributions in Fig. 15 show that the wall concentration remains zero for some distance downstream of the FSP, then rises rapidly to the fully mixed

value. The basic integral analysis was formulated with the assumption that the turbulent Schmidt number (S_{ct}) is unity. Computations for the C_t = 0.345 flow were also made with S_{ct} = 0.7 in the wake regimes; as shown by the dashed line in Fig. 15, this increase in the eddy diffusivity causes the predicted C_w to begin to rise at the FSP. But even with S_{ct} = 0.7, the predicted C_w distribution is in poor agreement with the experiment. Clearly, the axial diffusion of jet species upstream of the FSP is significant; of course, this streamwise turbulent diffusion is neglected in the basic integral analysis. The best that can be said of the predicted C_w distributions is that the fully mixed value is reached at approximately the correct axial station.

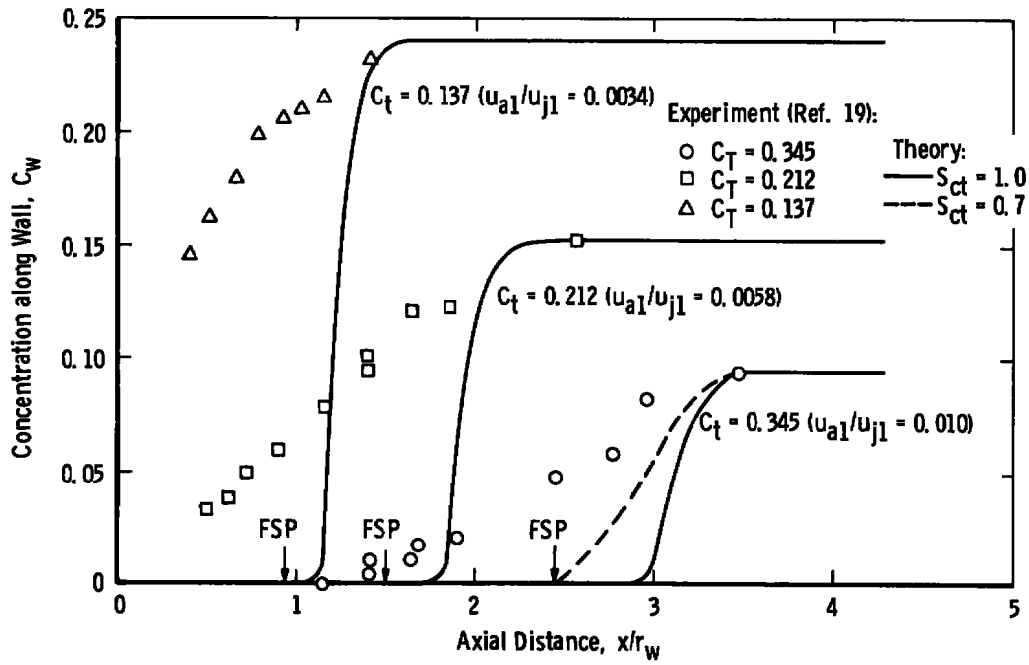

Figure 15. Wall concentration distribution for the experiments of Becker, et al.

The efficiency of a recirculation zone as a stirring device is strikingly demonstrated by the results shown in Fig. 15. For this geometry, reattachment does not begin until x/r_w is greater than four; therefore, the velocity field is very nonuniform for the axial distances shown in Fig. 15. On the other hand, the concentration profiles become uniform ($C_w = C_c$) at an axial station only about one duct radius downstream of the FSP. Of course, this observation is valid only for small values of r_n/r_w; for large values of r_n/r_w, such as investigated by Heskestad, the concentration profiles remain nonuniform at distances far downstream in the third regime.

3.4 EXPERIMENTS OF CHEDAILLE, ET AL.

Chedaille, Leuckel, and Chesters (Ref. 20) investigated an axisymmetric recirculating flow configuration that was similar to the one investigated by Becker, et al.; r_n/r_w was 0.031. However, Chedaille, et al., heated the jet to give T_{oj1}/T_{oa1} = 1.51 and made temperature measurements in the flow field. These temperature measurements permit tht distribution of jet species concentration in the flow field to be deduced.

Axial distributions of wall and centerline concentration are shown in Figs. 16a and b for two of the flows investigated by Chedaille, et al. Even though these flows involve density gradients, the experimental results are similar to those obtained by Becker, et al.

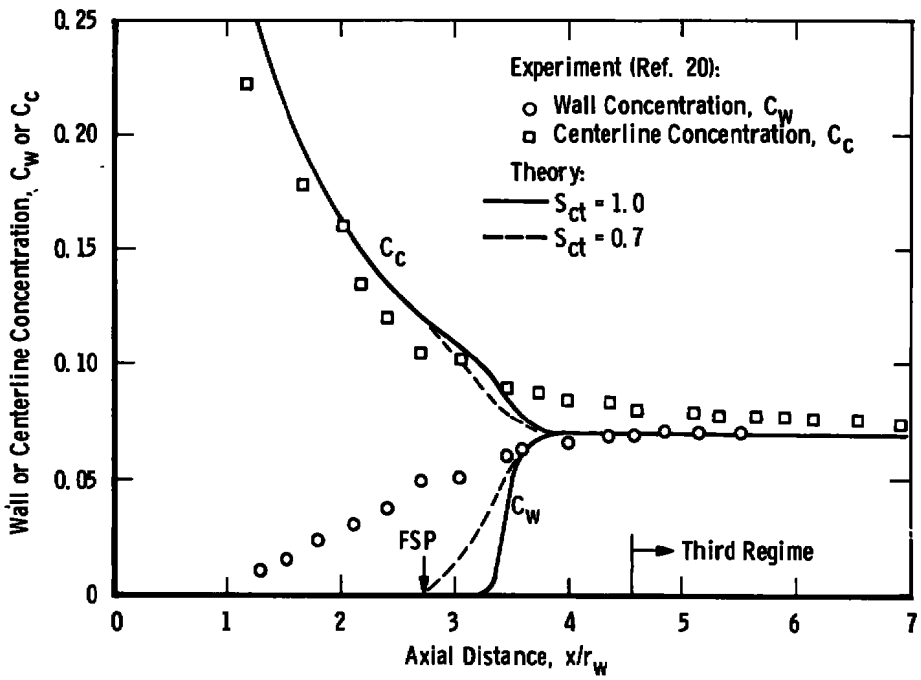

a. u_{a1}/u_{j1} = 0.0086, T_{oj}/T_{oa} = 1.51

Figure 16. Wall and centerline concentration distributions for the experiments of Chedaille, et al.

The C_w distribution begins to build up at an axial station well upstream of the FSP. However, C_w and C_c do not approach the fully mixed values as rapidly as for constant-density flow. The predicted results are qualitatively similar to those obtained for the Becker, et al., geometry. For S_{ct} = 1, C_w remains zero for some distance downsteam of the FSP, then rapidly rises to the fully mixed value. For S_{ct} = 0.7, the predicted C_w distribution begins to rise just downstream of the FSP.

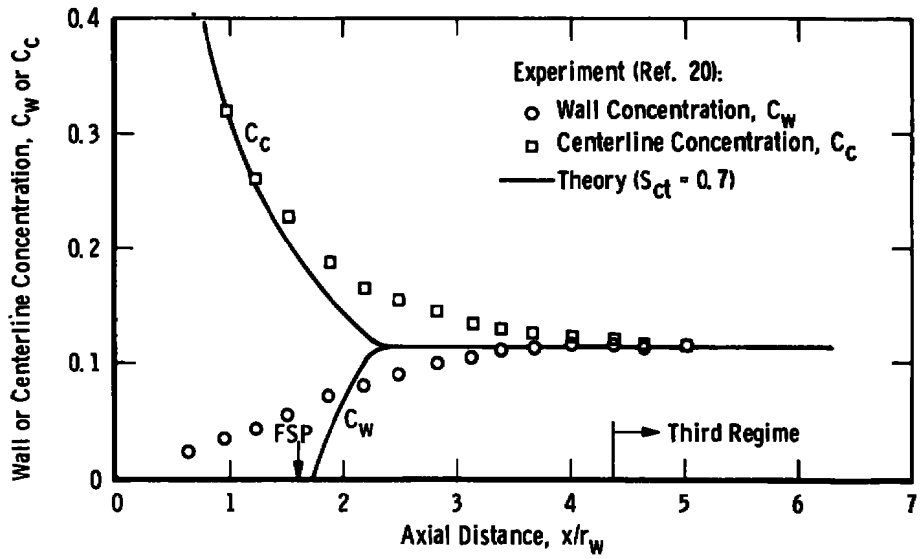

b. u_{a1}/u_{j1} = 0.0050, T_{oj}/T_{oa} = 1.51

Figure 16. Concluded.

3.5 COMPARISON WITH OTHER PREDICTIONS

In the limiting case of constant-density flow with a small value of r_n/r_w (nearly a point-source jet), the present integral analysis becomes similar to that of Hill (Ref. 11). The extent of recirculation predicted by the present analysis for the configuration of Barchilon and Curtet is shown in Fig. 17, along with Hill's prediction. The two predictions for the location of the FSP are nearly the same. However, Hill's analysis, which is based on a local model for the eddy viscosity, greatly overpredicts the distance to the RSP. The present theory would yield similar results if a local, rather than a frozen, eddy viscosity were used in the reattachment region.

The finite-difference elliptic analysis of Gosman, et al. (Ref. 8), was applied to the flow configuration of Barchilon and Curtet (C_t = 0.305). Lateral variations of the eddy viscosity were assumed to be negligible, and the axial distribution of the eddy viscosity was prescribed to be the same as that obtained in the basic integral analysis. Therefore, differences between the elliptic and integral solutions are attributable to the different governing equations and numerical procedures, rather than to different turbulent transport properties.

The axial distribution of centerline velocity predicted by the elliptic analysis (Fig. 18a) is in better agreement with experiment than is the prediction of the integral analysis. But the prediction of the integral analysis for the axial distribution of u_w is

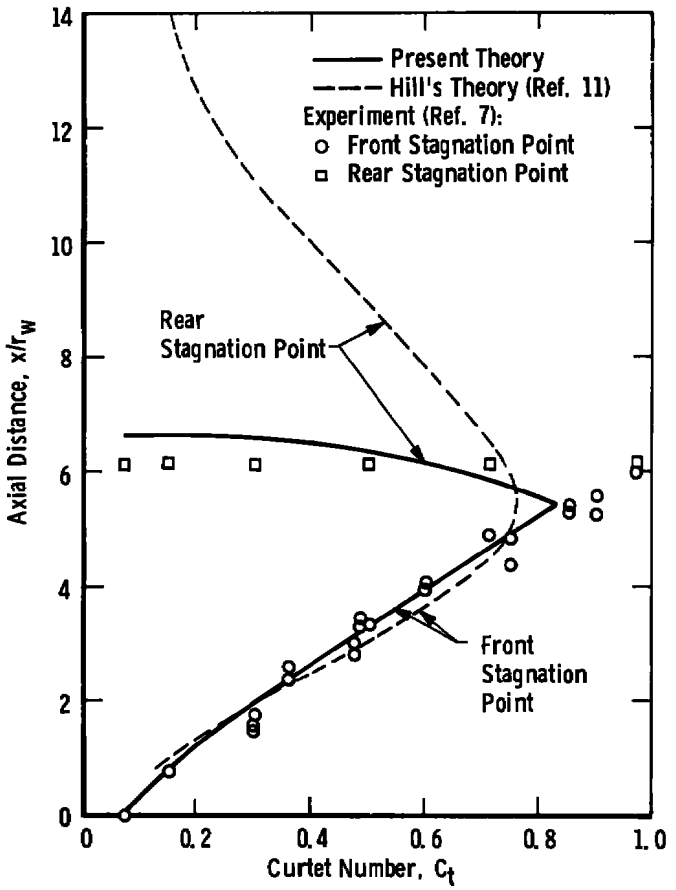

Figure 17. Comparison of present theory with Hill's results on extent of recirculation.

better than that of the elliptic analysis (Fig. 18b). The elliptic prediction of the location of the FSP is particularly poor. This result must be attributed to the numerical procedures or to the specification of the vorticity boundary conditions, because the flow upstream of the FSP is nearly parabolic and the eddy viscosity model used is realistic in this region. (Experience has shown that the location of the recirculation region predicted by the elliptic analysis can be significantly affected simply by changing either the computational mesh or the method of specifying the vorticity at the primary nozzle lip (Refs. 9 and 17.) In the present computations, these factors were selected after some trial and error to yield a good prediction of the centerline velocity distribution.)

In the computations, the Barchilon and Curtet flow was assumed to have tracer species in the primary fluid. Predicted axial distributions of the concentration of this

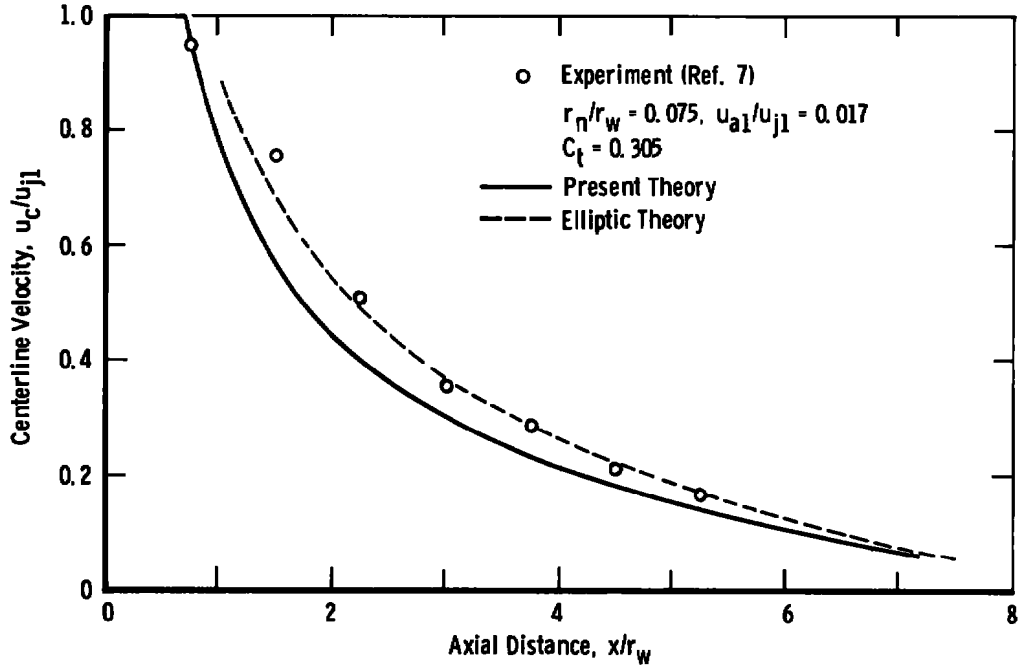

a. Centerline velocity distribution

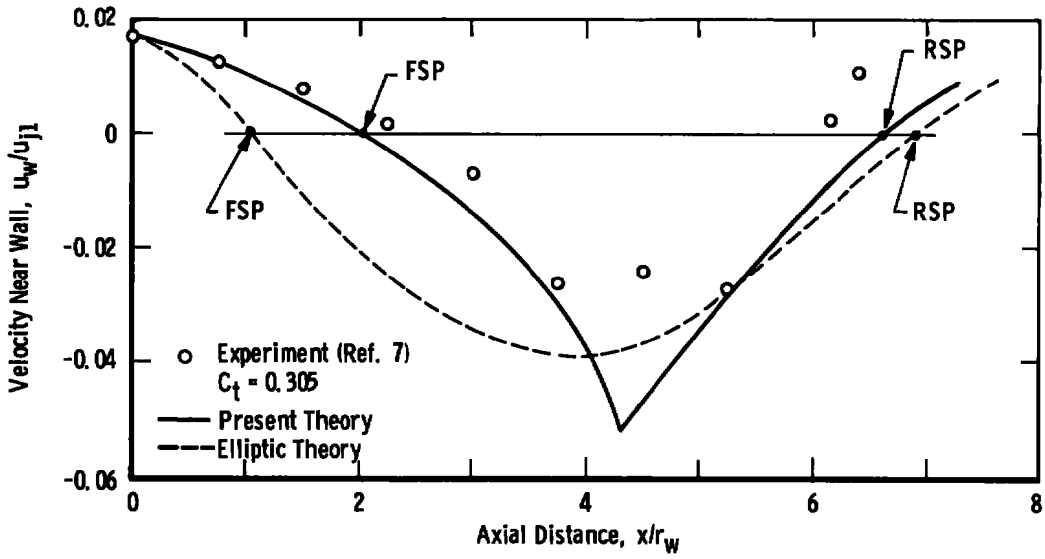

b. Velocity near wall

Figure 18. Comparison of integral theory and elliptic theory for the Barchilon and Curtet geometry.

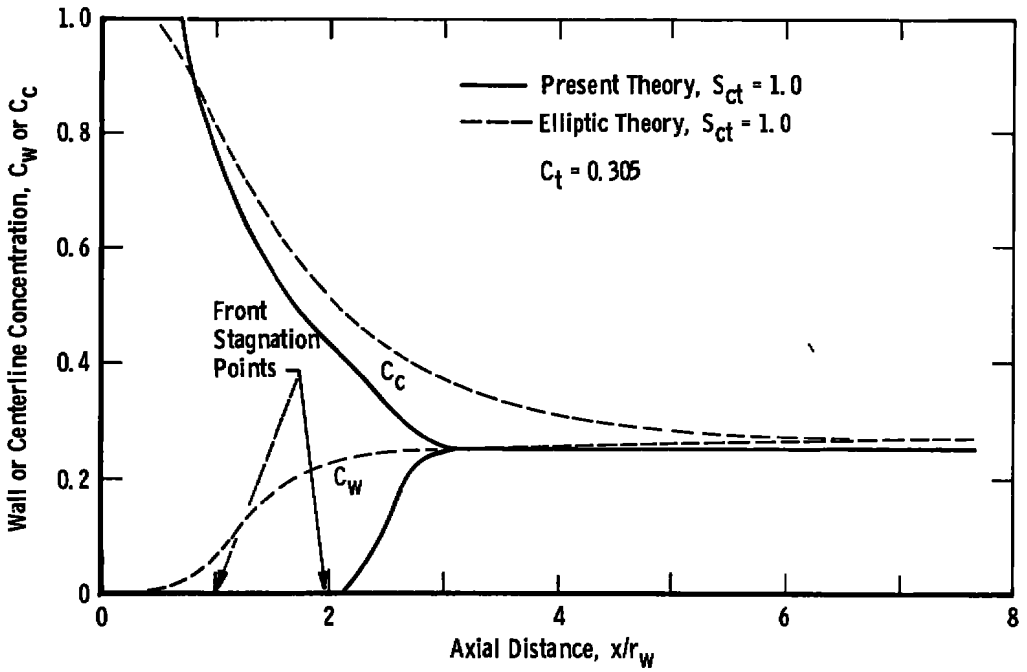

c. Wall and centerline concentration
Figure 18. Concluded.

tracer along the wall and along the centerline are shown in Fig. 18c. The elliptic solution yields the physically realistic result that C_w begins to increase upstream of the FSP. However, with the eddy viscosity model used, the computed counterstream diffusion of species along the wall is less than shown in the experiments of Becker, et al. (Note that the fully mixed concentration predicted by the elliptic analysis is higher than the correct value of 0.250. However, in this particular computation, the error is only about 10 percent.)

One of the major objectives of making the calculations with the Gosman program was to evaluate the species profile shape function that is used in the integral analysis. The relationship in the shear layer between the normalized concentration and the normalized velocity is shown in Figs. 19a through c. The integral and elliptic results are compared at equivalent values of u_w, rather that at equivalent axial stations. For flows without recirculation, the integral analysis predicts that the concentration profile parameter (K) remains nearly one (Fig. 19a). However, downstream of the FSP, K increases rapidly as the recirculation velocities become larger (Figs. 19b and c). The elliptic analysis also predicts a large distortion of the concentration profile relative to the velocity profile. So, even through the concentration profiles predicted by the two analyses are different in

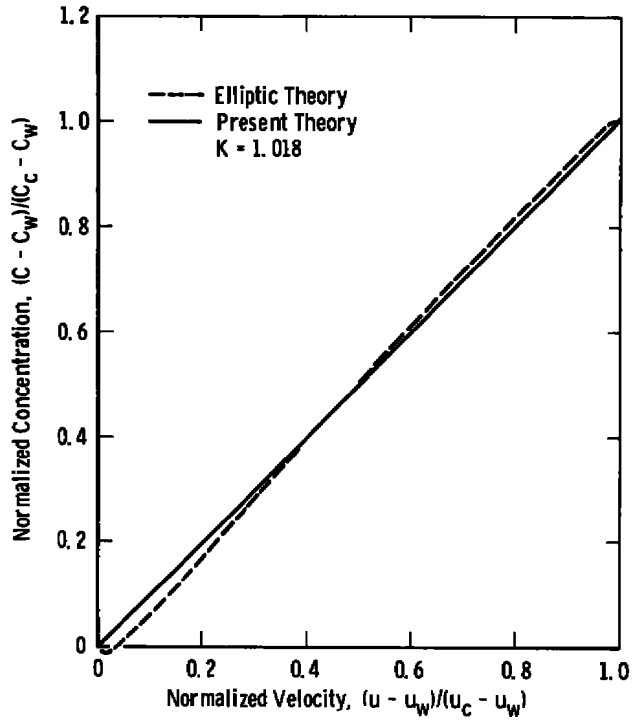

a. $u_w/u_{j1} = 0$

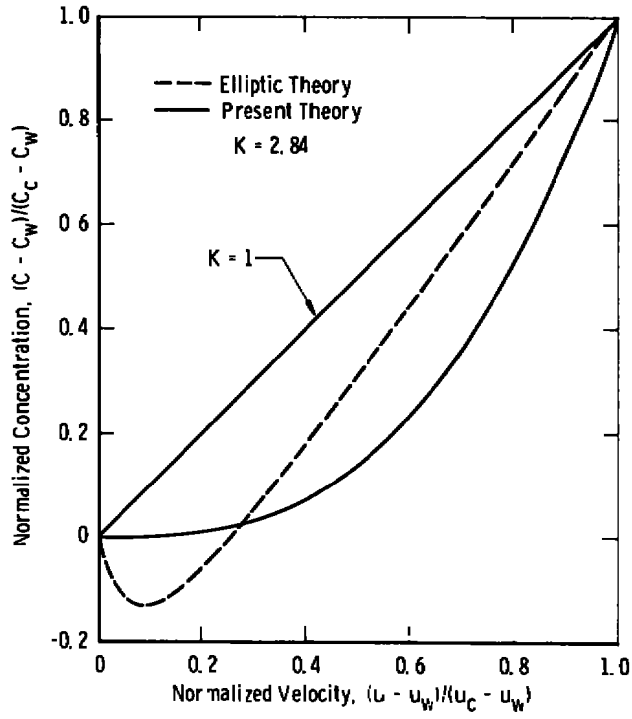

b. $u_w/u_{j1} = -0.012$

Figure 19. Concentration-velocity relationship for the Barchilon and Curtet geometry, $C_t = 0.305$.

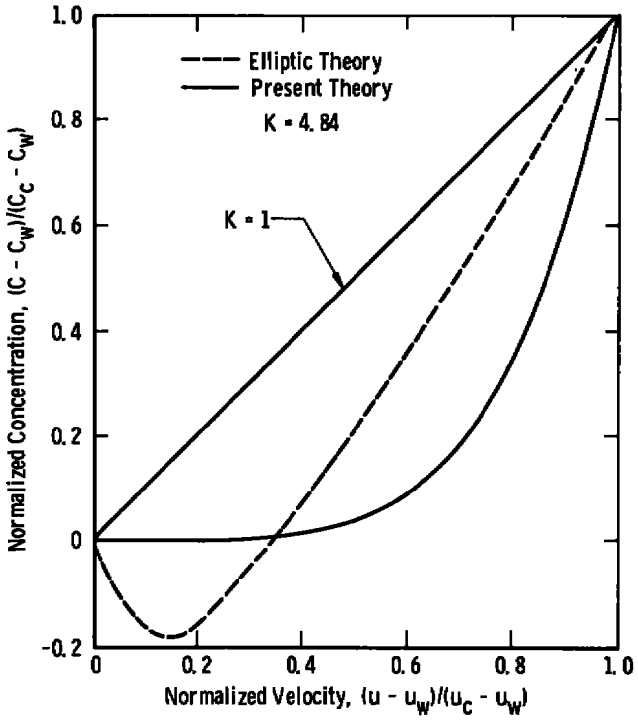

c. $u_w/u_{j1} = -0.018$

Figure 19. Concluded.

detail, one can conclude that the large distortion of the concentration profile predicted by the integral analysis is qualitatively correct.

3.6 DISCUSSION

The integral analysis shows that, for constant-density axisymmetric flows, the Curtet number is a very good correlating parameter for the occurrence of recirculation, even for r_n/r_w values much larger than are usually considered. Predicted limiting values of the initial velocity ratio (u_{a1}/u_{j1}) that just eliminate recirculation are shown in Fig. 20. Of course, the limiting velocity ratio depends strongly on r_n/r_w. But when the results are interpreted in terms of C_t, the limiting value of the Curtet number is seen to change by only 10 percent as r_n/r_w is increased from 0.02 to 0.50 (Fig. 21).

Based on the comparisons with experiment that have been presented, several conclusions can be drawn about the basic integral analysis of ducted flows with recirculation. First, the overall velocity field, including the location of the front and rear stagnation points, is fairly well predicted, at least for flows with small density gradients.

The major deficiency in the velocity predictions is the unrealistic cusp in the wall velocity distribution. The predicted concentration field is much less satisfactory than the predicted velocity field; a major deficiency in the analysis is the neglect of counterstream turbulent diffusion of species near the FSP. Note that, for the flows that have been considered, the density is uncoupled or is only weakly coupled to the concentration. Therefore, errors in the concentration field have only a small influence on the predicted velocity field. However, when the density is strongly coupled with the concentration, as it is in the hydrogen-air experiments of Schulz (Ref. 9) and Chriss (Ref. 21), the erroneously predicted concentration field can be expected to lead to significant errors in the predicted velocity field.

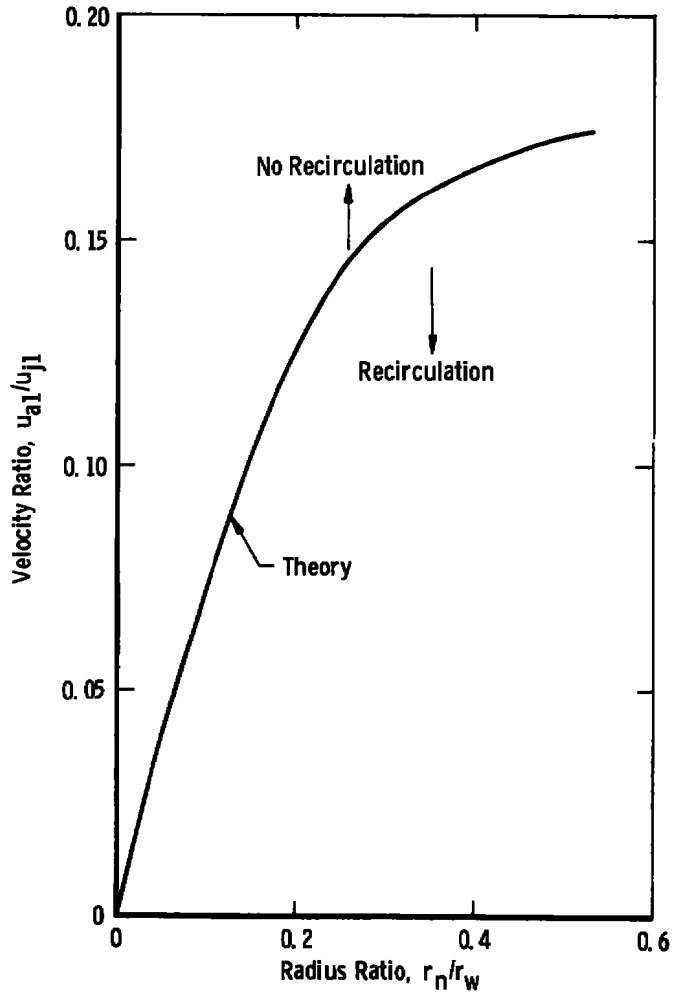

Figure 20. Limiting velocity ratio for recirculation in a constant-density flow within a cylindrical duct.

Clearly, the major deficiencies of the basic integral analysis are the neglect of streamwise diffusion of species (which is particularly important near the FSP) and the neglect of streamwise turbulent transport of momentum (which is particularly important near the beginning of reattachment). A deficiency of less importance is the neglect of the small but significant axial pressure gradients that occur between the FSP and the beginning of reattachment. An extended integral analysis, in which these deficiencies are avoided, is formulated in Section 4.0.

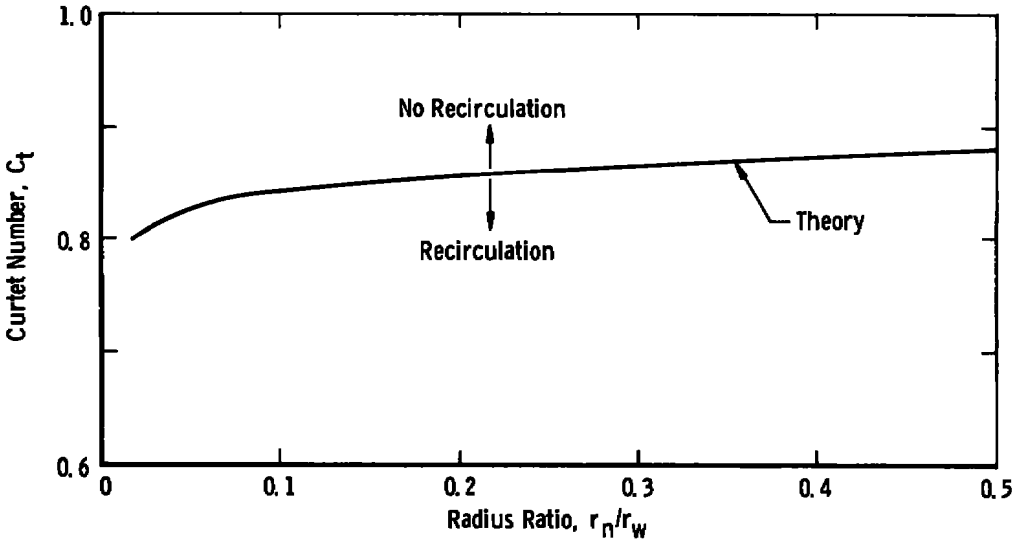

Figure 21. Limiting Curtet number for recirculation in a constant-density flow within a cylindrical duct.

4.0 FORMULATION OF EXTENDED INTEGRAL ANALYSIS

All of the assumptions used in formulating the basic analysis are retained in the extended analysis, with two exceptions. First, streamwise turbulent transport is not assumed to be negligible in the first wake, second wake, first wall and third regimes (The analysis of the first and second regimes is unchanged). Second, it is not assumed that the static pressure is constant in the first wake and second wake regimes; instead, the axial distribution of static pressure in these regimes will be computed.

4.1 BASIC EQUATIONS

The basic differential equations that describe the flow field are:

Continuity

$$\frac{\partial}{\partial x}(\rho u r^{\alpha}) + \frac{\partial}{\partial r}(\rho v r^{\alpha}) = 0 \qquad (1)$$

Axial Momentum

$$\rho u r^{\alpha} \frac{\partial u}{\partial x} + \rho v r^{\alpha} \frac{\partial u}{\partial r} = -r^{\alpha} \frac{\partial p}{\partial x} + \frac{\partial}{\partial r} (\tau r^{\alpha}) + \frac{\partial}{\partial x} (\sigma r^{\alpha}) \tag{32}$$

where τ is the turbulent shear stress and σ is the turbulent normal stress in the axial direction.

Element Species Conservation

$$\rho u r^{\alpha} \frac{\partial C}{\partial x} + \rho v r^{\alpha} \frac{\partial C}{\partial r} = \frac{\partial}{\partial r} (q r^{\alpha}) + \frac{\partial}{\partial r} (\beta r^{\alpha}) \tag{33}$$

where q is the lateral turbulent species flux and β is the turbulent species flux in the axial direction.

As in Section 2.3, Eqs. (1), (32), and (33) are integrated to obtain five integral equations:

Overall Continuity

$$\int_{r_c}^{r_w} \frac{\partial}{\partial x} (\rho u)\, r^{\alpha}\, dr = \rho_c u_c r_c^{\alpha} \frac{dr_c}{dx} - \rho_w u_w r_w^{\alpha} \frac{dr_w}{dx} \tag{5}$$

Overall Momentum

$$\int_{r_c}^{r_w} \frac{\partial}{\partial x} (\rho u^2)\, r^{\alpha}\, dr = \rho_c u_c^2 r_c^{\alpha} \frac{dr_c}{dx} - \rho_w u_w^2 r_w^{\alpha} \frac{dr_w}{dx} - \frac{\left[r_w^{\alpha+1} - r_c^{\alpha+1}\right]}{(\alpha + 1)} \frac{dp}{dx} + \int_{r_c}^{r_w} \frac{\partial}{\partial x} (\sigma)\, r^{\alpha}\, dr \tag{34}$$

Half-Radius Momentum

$$\int_{r_c}^{r_m} \frac{\partial}{\partial x} (\rho u^2)\, r^{\alpha}\, dr - u_m \int_{r_c}^{r_m} \frac{\partial}{\partial x} (\rho u)\, r^{\alpha}\, dr = r_m r_m^{\alpha} + (u_c - u_m)\, \rho_c u_c r_c^{\alpha} \frac{dr_c}{dx} - \frac{\left[r_m^{\alpha+1} - r_c^{\alpha+1}\right]}{(\alpha + 1)} \frac{dp}{dx} + \int_{r_c}^{r_m} \frac{\partial}{\partial x} (\sigma)\, r^{\alpha}\, dr \tag{35}$$

Overall Species

$$\int_{r_c}^{r_w} \frac{\partial}{\partial x} (\rho u C)\, r^{\alpha}\, dr = \rho_c u_c C_c r_c^{\alpha} \frac{dr_c}{dx} - \rho_w u_w C_w r_w^{\alpha} \frac{dr_w}{dx} + \int_{r_c}^{r_w} \frac{\partial}{\partial x} (\beta)\, r^{\alpha}\, dr \tag{36}$$

Half-Radius Species

$$\int_{r_c}^{r_m} \frac{\partial}{\partial x}(\rho u C)\, r^{\alpha}\, dr - C_m \int_{r_c}^{r_m} \frac{\partial}{\partial x}(\rho u)\, r^{\alpha} dr = q_m r_m^{\alpha} + \rho_c u_c (C_c - C_m) r_c^{\alpha} \frac{dr_c}{dx} + \int_{r_c}^{r_m} \frac{\partial}{\partial x}(\beta)\, r^{\alpha}\, dr \qquad (37)$$

Equations (34) through (37) are the same as Eqs. (6) through (9), except for the last term that appears on the right-hand side of each equation.

The static pressure is no longer assumed constant in the first-wake and second-wake regimes. Therefore, an additional equation must be introduced to permit the pressure to be calculated. The additional equation is chosen to be an axial momentum equation for the flow near the wall. Because τ and $\partial u/\partial r$ are assumed to be zero in this region, the wall momentum equation is:

$$\rho_w u_w \frac{du_w}{dx} = -\frac{dp}{dx} + \frac{d}{dx}(\sigma_w) \qquad (38)$$

4.2 STREAMWISE TRANSPORT TERMS

A gradient model of the streamwise transport processes is assumed. Therefore,

$$\sigma = \rho \epsilon \frac{\partial u}{\partial x} \qquad (39)$$

and

$$\beta = \rho \epsilon \frac{\partial C}{\partial x} \qquad (40)$$

where the eddy viscosity is assumed to be a function of only x; the eddy viscosity model is the same as that used in the basic integral analysis (Section 2.6).

With the gradient model for σ and β, the streamwise transport terms in Eqs. (34) through (38) contain second derivatives of u and C with respect to x. These second derivatives cause the system of equations to be elliptic in nature; of course, the solution techniques used for solving the integrated boundary layer equations are not applicable to this elliptic system. However, the solution techniques described in Sections 2.7 and 2.8 can be used if the streamwise transport terms are computed approximately.

Leibnitz' rule is applied to the streamwise transport integral terms that appear on the right-hand sides of Eqs. (34) through (37):

$$\int_{r_c}^{r_w} \frac{\partial}{\partial x}(\sigma) r^{\alpha} dr = \frac{d}{dx} \int_{r_c}^{r_w} \sigma r^{\alpha} dr - \sigma_w r_w^{\alpha} \frac{dr_w}{dx} + \sigma_c r_c^{\alpha} \frac{dr_c}{dx} \tag{41}$$

$$\int_{r_c}^{r_m} \frac{\partial}{\partial x}(\sigma) r^{\alpha} dr = \frac{d}{dx} \int_{r_c}^{r_m} \sigma r^{\alpha} dr - \sigma_m r_m^{\alpha} \frac{dr_m}{dx} + \sigma_c r_c^{\alpha} \frac{dr_c}{dx} \tag{42}$$

$$\int_{r_c}^{r_w} \frac{\partial}{\partial x}(\beta) r^{\alpha} dr = \frac{d}{dx} \int_{r_c}^{r_w} \beta r^{\alpha} dr - \beta_w r_w^{\alpha} \frac{dr_w}{dx} + \beta_c r_c^{\alpha} \frac{dr_c}{dx} \tag{43}$$

$$\int_{r_c}^{r_m} \frac{\partial}{\partial x}(\beta) r^{\alpha} dr = \frac{d}{dx} \int_{r_c}^{r_m} \beta r^{\alpha} dr - \beta_m r_m^{\alpha} \frac{dr_m}{dx} + \beta_c r_c^{\alpha} \frac{dr_c}{dx} \tag{44}$$

Now, we introduce the approximation that, at any x,

$$\frac{d}{dx} \int ( ) r^{\alpha} dr = \frac{1}{\Delta x} \int ( ) r^{\alpha} dr - \frac{1}{\Delta x} \left[\int ( ) r^{\alpha} dr \right]_{\ell} \tag{45}$$

where Δx is the computation step size and the subscript "ℓ" denotes a quantity evaluated at the last upstream computation station, (x - Δx). With Eq. (45) and the definitions of σ and β, Eqs. (41) through (44) become:

$$\int_{r_c}^{r_w} \frac{\partial}{\partial x}(\sigma) r^{\alpha} dr = \frac{\epsilon}{\Delta x} \int_{r_c}^{r_w} \rho \frac{\partial u}{\partial x} r^{\alpha} dr - \rho_w \epsilon r_w^{\alpha} \frac{dr_w}{dx} \frac{du_w}{dx} + \rho_c \epsilon r_c^{\alpha} \frac{dr_c}{dx} \frac{du_c}{dx} - \frac{1}{\Delta x} \left[\epsilon \int_{r_c}^{r_w} \rho \frac{\partial u}{\partial x} r^{\alpha} dr \right]_{\ell} \tag{46}$$

$$\int_{r_c}^{r_m} \frac{\partial}{\partial x}(\sigma) r^{\alpha} dr = \frac{\epsilon}{\Delta x} \int_{r_c}^{r_m} \rho \frac{\partial u}{\partial x} r^{\alpha} dr - \rho_m \epsilon r_m^{\alpha} \frac{dr_m}{dx} \frac{du_m}{dx} + \rho_c \epsilon r_c^{\alpha} \frac{dr_c}{dx} \frac{du_c}{dx} - \frac{1}{\Delta x} \left[\epsilon \int_{r_c}^{r_m} \rho \frac{\partial u}{\partial x} r^{\alpha} dr \right]_{\ell} \tag{47}$$

$$\int_{r_c}^{r_w} \frac{\partial}{\partial x}(\beta)\, r^{\alpha}\, dr = \frac{\epsilon}{\Delta x} \int_{r_c}^{r_w} \rho \frac{\partial C}{\partial x} r^{\alpha}\, dr - \rho_w \epsilon r_w^{\alpha} \frac{dr_w}{dx} \frac{dC_w}{dx}$$

$$+ \rho_c \epsilon r_c^{\alpha} \frac{dr_c}{dx} \frac{dC_c}{dx} - \frac{1}{\Delta x} \left[\epsilon \int_{r_c}^{r_w} \rho \frac{\partial C}{\partial x} r^{\alpha}\, dr \right]_{\ell} \tag{48}$$

$$\int_{r_c}^{r_m} \frac{\partial}{\partial x}(\beta)\, r^{\alpha}\, dr = \frac{\epsilon}{\Delta x} \int_{r_c}^{r_m} \rho \frac{\partial C}{\partial x} r^{\alpha}\, dr - \rho_m \epsilon r_m^{\alpha} \frac{dr_m}{dx} \frac{dC_m}{dx}$$

$$+ \rho_c \epsilon r_c^{\alpha} \frac{dr_c}{dx} \frac{dC_c}{dx} - \frac{1}{\Delta x} \left[\epsilon \int_{r_c}^{r_m} \rho \frac{\partial C}{\partial x} r^{\alpha}\, dr \right]_{\ell} \tag{49}$$

Similarly, the streamwise transport term on the right-hand side of Eq. (38) is approximated by

$$\frac{d}{dx}(\sigma_w) = \frac{1}{\Delta x} \rho_w \epsilon \frac{du_w}{dx} - \frac{1}{\Delta x} \left[\rho_w \epsilon \frac{du_w}{dx} \right]_{\ell} \tag{50}$$

In the first-wake, second-wake, and first-wall regimes, the terms in Eqs. (47) and (49) that contain dr_m/dx are nonlinear in the derivatives of the dependent variables. Therefore, in these regimes, dr_m/dx is approximated by $(dr_m/dx)_{\ell}$.

4.3 METHOD OF SOLUTION

With the approximate streamwise transport terms, Eqs. (5), (34), (35), (36), (37), and (38) can be transformed into a system of ordinary differential equations that is linear in the derivatives of the dependent variables. The transformation procedure is the same as used for the basic integral analysis.

First-wake regime - The flow is completely described by six variables (u_w, r_i, b, C_w, K, p). The resulting system of equations is

$$N_1 \frac{du_w}{dx} + N_2 \frac{dr_i}{dx} - N_3 \frac{db}{dx} + N_4 \frac{dC_w}{dx} + N_5 \frac{dK}{dx} + N_6 \frac{dp}{dx} = N_7 \tag{51}$$

where $N \equiv F^*$ for the continuity equation, $N \equiv G^*$ for the overall momentum equation, $N \equiv H^*$ for the half-radius momentum equation, $N \equiv I^*$ for the overall species equation, $N \equiv J^*$ for the half-radius species equation, and $N \equiv L^*$ for the wall momentum equation. The equations of the coefficients for all the regimes are presented in Appendix B.

Second-wake regime - The six dependent variables are (u_w, u_c, b, C_w, K, p), and the resulting system of equations is

$$N_1 \frac{du_w}{dx} + N_2 \frac{du_c}{dx} + N_3 \frac{db}{dx} - N_4 \frac{dC_w}{dx} - N_5 \frac{dK}{dx} + N_6 \frac{dp}{dx} = N_7 \tag{52}$$

Third regime - The wall momentum equation is not used in the third- or first-wall regimes. The five dependent variables are (u_w, u_c, p, C_w, K) and the system of equations is

$$N_1 \frac{du_w}{dx} + N_2 \frac{du_c}{dx} + N_3 \frac{dp}{dx} + N_4 \frac{dC_w}{dx} + N_5 \frac{dK}{dx} = N_6 \tag{53}$$

First-wall regime - The five dependent variables are (u_w, r_i, p, C_w, K), and the system of equations is

$$N_1 \frac{du_w}{dx} + N_2 \frac{dr_1}{dx} + N_3 \frac{dp}{dx} + N_4 \frac{dC_w}{dx} + N_5 \frac{dK}{dx} = N_6 \tag{54}$$

With the coefficients evaluated numerically, Eqs. (51) through (54) are solved with the same techniques that are used in the basic integral analysis.

4.4 INITIATION OF THE WAKE REGIMES

In order to account for the counterstream turbulent diffusion of species in the vicinity of the FSP, the first-wake or second-wake regime (whichever is appropriate for the particular flow) is initiated upstream of the FSP. Thus, the wake regime that is first encountered in a given flow is initiated with a positive value of u_w, rather than with $u_w = 0$ as in the basic analysis.

As the outer flow approaches the FSP, the velocity decreases toward zero. In a region just upstream of the FSP, the velocity is sufficiently low so that the turbulent motion in the recirculation region can propagate upstream. Thus, the appropriate wake regime must be initiated at the axial location where the approach velocity (u_a) is equal to an average turbulent fluctuation velocity (u′) in the outer flow.

The fluctuating velocity (u′) is calculated by assuming that the eddy viscosity in the outer flow is the same as in the shear layer at the particular axial station. But the eddy viscosity (ϵ) is the product of a turbulent velocity scale and a turbulent length scale (ℓ):

$$\epsilon = u' \ell \tag{55}$$

The length scale in the outer flow is assumed to be proportional to the width of the outer flow, that is, to $[r_w - (r_i + b)]$. With the eddy viscosity defined by Eq. (23), the turbulent velocity scale in the outer flow is described by

$$u' = \frac{k\, b \left| u_c - u_a \right|}{c \left[r_w - (r_i + b) \right]} \tag{56}$$

where c is a prescribed constant, which should be about one. At each axial station in the first and second regime computations, u_a is compared with u' obtained from Eq. (56). The appropriate wake regime is initiated when $u_a = u'$.

4.5 DISCUSSION OF THE EXTENDED ANALYSIS

Although streamwise transport terms have been included in the momentum and species conservation equations, the analysis must be considered at best only "quasi-elliptic," since it was developed only to compute approximately the locally elliptic regions in flows that are grossly parabolic. Because of the assumptions in the analysis, the downstream boundary conditions are implied to be only weakly coupled to the recirculation region. That is, the duct must have no abrupt changes in cross-sectional area, and must be long enough so that the flow downstream of the RSP approaches the fully mixed condition. In essence, the downstream boundary conditions are assumed to be isolated from the elliptic region by a region of parabolic flow.

5.0 CONCLUDING REMARKS

The basic integral analysis, which involves the solution of the integral form of the boundary-layer equations, is computationally efficient and yields results that are sufficiently accurate for many purposes. Indeed, the predictions for the location and extent of recirculation in ducted flows are very good, at least for flows with moderate density gradients. But the streamwise turbulent transport terms, which are neglected in the basic analysis, are important in establishing the concentration field near the front stagnation point and in establishing the velocity field near the onset of reattachment.

In the extended integral analysis, which has been programmed for numerical solution, the streamwise transport terms have been included in an approximate manner. The validity of this quasi-elliptic analysis must be established by comparison with the available experimental results on constant-density and variable-density ducted flows with recirculation.

The eddy viscosity model used in this study yields satisfactory results for the flows considered. But for complex variable-density flows, such as occur in combustion systems, the simple eddy viscosity model can be expected to be unsatisfactory. A more

sophisticated turbulence model, based on solution of the turbulent kinetic energy (TKE) equation, will be required for complex flows. For flows without recirculation, the present integral analysis has already been extended to include solution of an integrated TKE eqution for the shear layer (Ref. 22).

REFERENCES

1. Edelman, R. B. and Fortune, O. "An Analysis of Mixing and Combustion in Ducted Flows." AIAA Paper No. 68-114, January 1968.

2. Peters, C. E. "Turbulent Mixing and Burning of Coaxial Streams inside a Duct of Arbitrary Shape." AEDC-TR-68-270 (AD680397), Janaury 1969.

3. Peters, C. E., Phares, W. J., and Cunningham, T.H.M. "Theoretical and Experimental Studies of Ducted Mixing and Burning of Coaxial Streams." Journal of Spacecraft and Rockets, Vol. 6, No. 12, December 1969, pp. 1435-1441.

4. Hill, P. G. "Turbulent Jets in Ducted Streams." Journal of Fluid Mechanics, Vol. 22, Part 1, 1965, pp. 161-186.

5. Mikhail, S. "Mixing of Coaxial Streams Inside a Closed Conduit." Journal of Mechanical Engineering Science, Vol. 2, No. 1, March 1960, pp. 59-68.

6. Smoot, L. D., et al. "A Model for Mixing and Combustion in Particle-Laden Ducted Flows." AIAA Paper No. 70-736, June 1970.

7. Barchilon, M. and Curtet, R. "Some Details of the Structure of an Axisymmetric Confined Jet with Backflow." Transactions of the ASME, Journal of Basic Engineering, Vol. 86, December 1964, pp. 777-787.

8. Gosman, A. D., et al. Heat and Mass Transfer in Recirculating Flows. Academic Press, New York, 1969.

9. Schulz, R. J. "An Investigation of Ducted, Two-Stream, Varible-Density, Turbulent Jet Mixing with Recirculation." AEDC-TR-76-152(AFOSR-TR-76-1087) (ADA034537), January 1977.

10. Edelman, R. B. and Harsha, P. T. "Analytical Modeling of Sudden Expansion Burners." CPIA Publication No. 287, June 1977.

11. Hill, P. G. "Incompressible Jet Mixing in Converging-Diverging Axisymmetric Ducts." Transactions of the ASME, Journal of Basic Engineering, Vol. 89, March 1967, pp. 210-220.

12. Schubauer, G. B. and Tchen, C. M. "Turbulent Flow." In High Speed Aerodynamics and Jet Propulsion, Volume V, Turbulent Flows and Heat Transfer, edited by C. C. Lin, Princeton University Press, 1959, p. 171.

13. Phares, W. J. and Loper, F. C. "A Technique for Solving Integro-Differential Equations with Application to Turbulent Mixing." AEDC-TR-64-209 (AD450730), November 1964.

14. Thring, M. W. and Newby, M. P. "Combustion Length of Enclosed Turbulent Jet Flames." In Proceedings of of the Fourth Symposium (International) on Combustion, Williams and Wilkins, London, 1953, pp. 789-796.

15. Curtet, R. "Confined Jets and Recirculation Phenomena with Cold Air." Combustion and Flame, Vol. 2, No. 2, October-December 1958, pp. 383-411.

16. Becker, H. A., Hottel, H. C., and Williams, G. C. "Mixing and Flow in Ducted Turbulent Jets." In Ninth Symposium (International) on Combustion, Academic Press, New York, 1963, pp. 7-20.

17. Schulz, R. J. "An Experimental and Theoretical Investigation of Confined, Two-Stream, Variable-Density, Turbulent Jet Mixing with Recirculation." PhD Dissertation, University of Tennessee, June 1976.

18. Heskestad, G. "Further Experiments with Suction at a Sudden Enlargement in a Pipe." Transactions of the ASME, Journal of Basic Engineering, Vol. 92, No. 3, September 1970, pp. 437-449.

19. Becker, H. A., Hottel, H. C., and Williams, G. C. "Concentration Intermittency in Jets." In Proceedings of the Tenth Symposium (International) on Combustion, Academic Press, New York, 1965, pp. 1253-1263.

20. Chedaille, J., Leuckel, W., and Chesters, A. K. "Aerodynamic Studies Carried out on Turbulent Jets by the International Flame Research Foundation." Journal of the Institute of Fuel, Vol. 39, December 1966, pp. 506-520.

21. Chriss, D. E. "An Experimental Investigation of Ducted, Reactive, Turbulent Jet Mixing with Recirculation." AEDC-TR-77-56(AFOSR-TR-77-0749) (ADA044110), September 1977.

22. Peters, C. E. and Phares, W. J. "An Integral Turbulent Kinetic Energy Analysis of Free Shear Flows." In Free Turbulent Shear Flows, Volume I, Conference Proceedings, NASA SP 321, 1973, pp. 577-624.

APPENDIX A
COEFFICIENTS FOR THE BASIC INTEGRAL ANALYSIS

The following parameters are defined:

$$y = (r - r_i)/b$$

$$r^{\alpha}\,dr = \alpha b^2 y\,dy + r_i^{\alpha} b\,dy\,; \quad \alpha = 0 \text{ or } 1$$

$$S_{1z_k} = \frac{\partial}{\partial z_k}(\rho u)$$

$$S_{2z_k} = \frac{\partial}{\partial z_k}(\rho u^2)$$

$$S_{3z_k} = \frac{\partial}{\partial z_k}(\rho uC)$$

$$S_{4z_k} = \rho \frac{\partial}{\partial z_k}(u)$$

$$S_{5z_k} = \rho \frac{\partial}{\partial z_k}(C)$$

where z_k is a generalized variable.

The first and second regime coefficients (F, G, H, and I) are:

$$F_1 = \alpha b^2 \int_0^1 S_{1z_1}\,y\,dy + r_i^{\alpha} b \int_0^1 S_{1z_1}\,dy + \frac{\left(r_i^{\alpha+1} - r_c^{\alpha+1}\right)}{(\alpha+1)} \frac{d}{dp}(\rho_j u_j) + \left[\frac{\bar{r}_w^{\alpha+1} - (r_i + b)^{\alpha+1}}{\alpha+1}\right] \frac{d}{dp}(\rho_a u_a)$$

$$F_2 = \alpha b^2 \int_0^1 S_{1z_2}\,y\,dy + r_i^{\alpha} b \int_0^1 S_{1z_2}\,dy$$

$$F_3 = \alpha b^2 \int_0^1 S_{1z_3}\,y\,dy - r_i^{\alpha} b \int_0^1 S_{1z_3}\,dy$$

$$F_4 = ab^2 \int_0^1 S_{1z_4}\, y\,dy + r_i^a b \int_0^1 S_{1z_4}\, dy$$

$$F_5 = -ab^2 \int_0^1 S_{1z_5}\, y\,dy - r_i^a b \int_0^1 S_{1z_5}\, dy - \rho_a u_a r_w^a \frac{dr_w}{dx} - \rho_c u_c r_c^a \frac{dr_c}{dx}$$

$$G_1 = ab^2 \int_0^1 S_{2z_1}\, y\,dy + r_i^a b \int_0^1 S_{2z_1}\, dy + \left(\frac{r_i^{a+1} - r_c^{a-1}}{a+1}\right) \frac{d}{dp}\left(\rho_j u_j^2\right) + \left[\frac{r_w^{a+1} - (r_i + b)^{a+1}}{a+1}\right] \frac{d}{dp}\left(\rho_a u_a^2\right) + \left(\frac{r_w^{a+1} - r_c^{a+1}}{a+1}\right)$$

$$G_2 = ab^2 \int_0^1 S_{2z_2}\, y\,dy + r_i^a b \int_0^1 S_{2z_2}\, dy$$

$$G_3 = ab^2 \int_0^1 S_{2z_3}\, y\,dy + r_i^a b \int_0^1 S_{2z_3}\, dy$$

$$G_4 = ab^2 \int_0^1 S_{2z_4}\, y\,dy + r_i^a b \int_0^1 S_{2z_4}\, dy$$

$$G_5 = -ab^2 \int_0^1 S_{2z_5}\, y\,dy - r_i^a b \int_0^1 S_{2z_5}\, dy - \rho_a u_a^2 r_w^a \frac{dr_w}{dx} + \rho_c u_c^2 r_c^a \frac{dr_c}{dx} + r_w^a r_w$$

$$H_1 = ab^2 \int_0^{1/2} S_{2z_1}\, y\,dy - r_i^a b \int_0^{1/2} S_{2z_1}\, dy - u_m ab^2 \int_0^{1/2} S_{1z_1}\, y\,dy - u_m r_i^a b \int_0^{1/2} S_{1z_1}\, dy - \left(\frac{r_i^{a-1} - r_c^{a+1}}{a+1}\right) \left[\frac{d}{dp}\left(\rho_j u_j^2\right) - u_m \frac{d}{dp}\left(\rho_j u_j\right)\right] - \left(\frac{r_m^{a+1} - r_c^{a+1}}{a+1}\right)$$

$$H_2 = ab^2 \int_0^{1/2} S_{2z_2}\, y\,dy + r_i^a b \int_0^{1/2} S_{2z_2}\, dy - u_m ab^2 \int_0^{1/2} S_{1z_2}\, y\,dy - u_m r_i^a b \int_0^{1/2} S_{1z_2}\, dy$$

$$H_3 = ab^2 \int_0^{1/2} S_{2z_3}\, ydy + r_i^a b \int_0^{1/2} S_{2z_3}\, dy - u_m\, ab^2 \int_0^{1/2} S_{1z_3}\, ydy - u_m r_i^a b \int_0^{1/2} S_{1z_3}\, dy$$

$$H_4 = ab^2 \int_0^{1/2} S_{2z_4}\, ydy + r_i^a b \int_0^{1/2} S_{2z_4}\, dy - u_m\, ab^2 \int_0^{1/2} S_{1z_4}\, ydy - u_m r_i^a b \int_0^{1/2} S_{1z_4}\, dy$$

$$H_5 = -ab^2 \int_0^{1/2} S_{2z_5}\, ydy - r_i^a b \int_0^{1/2} S_{2z_5}\, ydy + u_m\, ab^2 \int_0^{1/2} S_{1z_5}\, ydy$$

$$+ u_m r_i^a b \int_0^{1/2} S_{1z_5}\, dy + r_m r_m^a - (u_c - u_m)\, \rho_c u_c r_c^a \frac{dr_c}{dx}$$

$$I_1 = \left(\frac{r_i^{a+1} - r_c^{a+1}}{a+1}\right) \frac{a}{dp}\,(\rho_j u_j) + ab^2 \int_0^1 S_{3z_1}\, ydy - r_i^a b \int_0^1 S_{3z_1}\, dy$$

$$I_2 = ab^2 \int_0^1 S_{3z_2}\, ydy + r_i^a b \int_0^1 S_{3z_2}\, dy$$

$$I_3 = ab^2 \int_0^1 S_{3z_3}\, ydy - r_i^a b \int_0^1 S_{3z_3}\, dy$$

$$I_4 = ab^2 \int_0^1 S_{3z_4}\, ydy + r_i^a b \int_0^1 S_{3z_4}\, dy$$

$$I_5 = -ab^2 \int_0^1 S_{3z_5}\, ydy - r_i^a b \int_0^1 S_{3z_5}\, dy + \rho_c u_c C_c r_c^a \frac{dr_c}{dx}$$

In the first regime (where $\rho_c = \rho_j$, $u_c = u_j$ and $C_c = 1$), $z_1 = p$, $z_2 = r_i$, $z_3 = b$, $z_4 = K$, and $z_5 = x$. In the second regime (where $r_i = r_c$), $z_1 = p$, $z_2 = u_c$, $z_3 = b$, $z_4 = k$, and $z_5 = x$.

The third, first wake, second wake and first wall regime coefficients (F, G, H, I, and J) are:

$$F_1 = ab^2 \int_0^1 S_{1z_1}\, y\,dy + r_i^a b \int_0^1 S_{1z_1}\, dy + \left[\frac{r_w^{a+1} - (r_i + b)^{a+1}}{a+1}\right] \frac{\partial}{\partial u_w} (\rho_w u_w)$$

$$F_2 = ab^2 \int_0^1 S_{1z_2}\, y\,dy + r_i^a b \int_0^1 S_{1z_2}\, dy$$

$$F_3 = ab^2 \int_0^1 S_{1z_3}\, y\,dy + r_i^a b \int_0^1 S_{1z_3}\, dy + \delta \left(\frac{r_i^{a+1} - r_c^{a-1}}{a+1}\right) \frac{d}{dp} (\rho_j u_j)$$

$$F_4 = ab^2 \int_0^1 S_{1z_4}\, y\,dy - r_i^a b \int_0^1 S_{1z_4}\, dy - \left(\frac{r_w^{a+1} - (r_i + b)^{a+1}}{a+1}\right) \frac{\partial}{\partial C_w} (\rho_w u_w)$$

$$F_5 = ab^2 \int_0^1 S_{1z_5}\, y\,dy + r_i^a b \int_0^1 S_{1z_5}\, dy$$

$$F_6 = -ab^2 \int_0^1 S_{1z_6}\, y\,dy - r_i^a b \int_0^1 S_{1z_6}\, dy - \rho_w u_w r_w^a \frac{dr_w}{dx} + \rho_c u_c r_c^a \frac{dr_c}{dx}$$

$$G_1 = ab^2 \int_0^1 S_{2z_1}\, y\,dy - r_i^a b \int_0^1 S_{2z_1}\, dy + \left(\frac{r_w^{a+1} - (r_i + b)^{a+1}}{a+1}\right) \frac{\partial}{\partial u_w} (\rho_w u_w^2)$$

$$G_2 = ab^2 \int_0^1 S_{2z_2}\, y\,dy + r_i^a b \int_0^1 S_{2z_2}\, dy$$

$$G_3 = ab^2 \int_0^1 S_{2z_3}\, y\,dy + r_i^a b \int_0^1 S_{2z_3}\, dy + \delta \left(\frac{r_w^{a+1} - r_c^{a+1}}{a+1}\right) + \delta \left(\frac{r_i^{a+1} - r_c^{a+1}}{a+1}\right) \frac{d}{dp} (\rho_j u_j^2)$$

$$G_4 = ab^2 \int_0^1 S_{2z_4}\, y\,dy - r_i^a b \int_0^1 S_{2z_4}\, dy + \left(\frac{r_w^{a+1} - (r_i - b)^{a-1}}{a+1}\right) \frac{\partial}{\partial G_w} (\rho_w u_w^2)$$

$$G_5 = ab^2 \int_0^1 S_{2z_5}\, y\,dy - r_i^a b \int_0^1 S_{2z_5}\, dy$$

$$G_6 = -ab^2 \int_0^1 S_{2z_6}\, y\,dy - r_i^a b \int_0^1 S_{2z_6}\, dy - \rho_w u_w^2 r_w^a \frac{dr_w}{dx} + \rho_c u_c^2 r_c^a \frac{dr_c}{dx}$$

$$H_1 = ab^2 \int_0^{1/2} S_{2z_1}\, y\,dy + r^a b \int_0^{1/2} S_{2z_1}\, dy - u_m ab^2 \int_0^{1/2} S_{1z_1}\, y\,dy - u_m r_i^a b \int_0^1 S_{1z_1}\, dy$$

$$H_2 = ab^2 \int_0^{1/2} S_{2z_2}\, y\,dy + r_i^a b \int_0^{1/2} S_{2z_2}\, dy - u_m ab^2 \int_0^{1/2} S_{1z_2}\, y\,dy - u_m r_i^a b \int_0^{1/2} S_{1z_2}\, dy$$

$$H_3 = ab^2 \int_0^{1/2} S_{2z_3}\, y\,dy + r_i^a b \int_0^{1/2} S_{2z_3}\, dy - u_m ab^2 \int_0^{1/2} S_{1z_3}\, y\,dy$$

$$- u_m r_i^a b \int_0^{1/2} S_{1z_3}\, dy + \delta \left(\frac{r_m^{a+1} - r_c^{a+1}}{a+1}\right) + \delta \left(\frac{r_i^{a+1} - r_c^{a+1}}{a+1}\right) \frac{d}{dp} (\rho_j u_j^2)$$

$$- \delta u_m \left(\frac{r_i^{a+1} - r_c^{a+1}}{a-1}\right) \frac{d}{dp} (\rho_j u_j)$$

$$H_4 = ab^2 \int_0^{1/2} S_{2z_4}\, y\,dy + r_i^a b \int_0^{1/2} S_{2z_4}\, dy - u_m ab^2 \int_0^{1/2} S_{1z_4}\, y\,dy - u_m ab^2 \int_0^{1/2} S_{1z_4}\, dy$$

$$H_5 = ab^2 \int_0^{1/2} S_{2z_5}\, y\,dy + r_i^a b \int_0^{1/2} S_{2z_5}\, dy - u_m ab^2 \int_0^1 S_{1z_5}\, y\,dy - u_m r_i^a b \int_0^{1/2} S_{1z_5}\, dy$$

$$H_6 = -ab^2 \int_0^{1/2} S_{2z_6}\, ydy - r_i^a b \int_0^{1/2} S_{2z_6}\, dy + u_m\, ab^2 \int_0^{1/2} S_{1z_6}\, ydy$$

$$+ u_m\, r_i^a\, b \int_0^{1/2} S_{1z_6}\, dy + r_m\, r_m^a + \rho_c u_c\, r_c^a\, \frac{dr_c}{dx}\, (u_c - u_m)$$

$$I_1 = ab^2 \int_0^{1} S_{3z_1}\, ydy - r_i^a b \int_0^{1} S_{3z_1}\, dy + \left(\frac{r_w^{a+1} - (r_i + b)^{a+1}}{a - 1}\right) \frac{\partial}{\partial u_w}\, (\rho_w u_w C_w)$$

$$I_2 = ab^2 \int_0^{1} S_{3z_2}\, ydy + r_i^a\, b \int_0^{1} S_{3z_2}\, dy$$

$$I_3 = ab^2 \int_0^{1} S_{3z_3}\, ydy + r_i^a\, b \int_0^{1} S_{3z_3}\, dy + \delta \left(\frac{r_i^{a+1} - r_c^{a+1}}{a + 1}\right) \frac{d}{dp}\, (\rho_j u_j)$$

$$I_4 = ab^2 \int_0^{1} S_{3z_4}\, ydy - r_i^a\, b \int_0^{1} S_{3z_4}\, dy - \left(\frac{r_w^{a+1} - (r_i + b)^{a+1}}{a + 1}\right) \frac{\partial}{\partial C_w}\, (\rho_w u_w C_w)$$

$$I_5 = ab^2 \int_0^{1} S_{3z_5}\, ydy + r_i^a\, b \int_0^{1} S_{3z_5}\, dy$$

$$I_6 = -ab^2 \int_0^{1} S_{3z_6}\, ydy - r_i^a\, b \int_0^{1} S_{3z_6}\, dy - \rho_c u_c C_c r_c^a\, \frac{dr_c}{dx} - \rho_w u_w C_w r_w^a\, \frac{dr_w}{dx}$$

$$J_1 = ab^2 \int_0^{1/2} S_{3z_1} ydy + r_i^a\, b \int_0^{1/2} S_{3z_1}\, dy$$

$$- C_m\, ab^2 \int_0^{1/2} S_{1z_1}\, ydy - C_m r_i^a\, b \int_0^{1/2} S_{1z_1}\, dy$$

$$J_2 = ab^2 \int_0^{1/2} S_{3z_2}\, ydy + r_i^a b \int_0^{1/2} S_{3z_2}\, dy - C_m ab^2 \int_0^{1/2} S_{1z_2}\, ydy - C_m r_i^a b \int_0^{1/2} S_{1z_2}\, dy$$

$$J_3 = ab^2 \int_0^{1/2} S_{3z_3}\, ydy + r_i^a b \int_0^{1/2} S_{3z_3}\, dy - C_m ab^2 \int_0^{1/2} S_{1z_3}\, ydy - C_m r_i^a b \int_0^{1/2} S_{1z_3}\, dy + \delta (1 - C_m) \left(\frac{r_i^{a+1} - r_c^{a+1}}{a+1} \right) \frac{d}{dp} (\rho_j u_j)$$

$$J_4 = ab^2 \int_0^{1/2} S_{3z_4}\, ydy + r_i^a b \int_0^{1/2} S_{3z_4}\, dy - C_m ab^2 \int_0^{1/2} S_{1z_4}\, ydy - C_m r_i^a b \int_0^{1/2} S_{1z_4}\, dy$$

$$J_5 = ab^2 \int_0^{1/2} S_{3z_5}\, ydy + r_i^a b \int_0^{1/2} S_{3z_5}\, dy - C_m ab^2 \int_0^{1/2} S_{1z_5}\, ydy - C_m r_i^a b \int_0^{1/2} S_{1z_5}\, dy$$

$$J_6 = -ab^2 \int_0^{1/2} S_{3z_6}\, ydy - r_i^a b \int_0^{1/2} S_{3z_6}\, dy + C_m ab^2 \int_0^{1/2} S_{1z_6}\, ydy + C_m r_i^a b \int_0^{1/2} S_{1z_6}\, dy + \rho_c u_c (C_c - C_m) r_c^a \frac{dr_c}{dx} + q_m r_m^a$$

In the third regime (where $r_i = r_c$, $b = r_w - r_c$, and $\delta = 1$), $z_1 = u_w$, $z_2 = u_c$, $z_3 = p$, $z_4 = C_w$, $z_5 = K$, and $z_6 = x$.

In the first-wake regime, $z_1 = u_w$, $z_2 = r_i$, $z_3 = b$, $z_4 = C_w$, $z_5 = K$, and $z_6 = x$ (the pressure is constant in this regime; therefore $\delta = 0$).

In the second-wake regime (where $r_i = r_c$), $z_1 = u_w$, $z_2 = u_c$, $z_3 = b$, $z_4 = C_w$, $z_5 = K$, and $z_6 = x$ (the pressure is constant in this regime; therefore $\delta = 0$).

In the first-wall regime (where $b = r_w - r_i$ and $\delta = 1$), $z_1 = u_w$, $z_2 = r_i$, $z_3 = p$, $z_4 = C_w$, $z_5 = K$, and $z_6 = x$.

APPENDIX B
COEFFICIENTS FOR THE EXTENDED INTEGRAL ANALYSIS

The parameters defined in Appendix A are also used in this appendix. Whenever possible, the coefficients are written as the basic analysis coefficients with additional terms as required.

In the first-wake and second-wake regimes, the coefficients (F*, G*, H*, I*, J*, L*) are:

$$F_1^* = F_1$$

$$F_2^* = F_2$$

$$F_3^* = F_3$$

$$F_4^* = F_4$$

$$F_5^* = F_5$$

$$F_6^* = ab^2 \int_0^1 S_{1z_6}\, y\,dy + r_i^a b \int_0^1 S_{1z_6}\, dy + \frac{\left(r_i^{a+1} - r_c^{a+1}\right)}{(a+1)} \frac{d}{dp}\left(\rho_j u_j\right) + \frac{\left[r_w^{a+1} - (r_i + b)^{a+1}\right]}{(a+1)} u_w \frac{\partial \rho_w}{\partial p}$$

$$F_7^* = F_6$$

$$G_1^* = G_1 - ab^2 \frac{\epsilon}{\Delta x} \int_0^1 S_{4z_1}\, y\,dy - r_i^a b \frac{\epsilon}{\Delta x} \int_0^1 S_{4z_1}\, dy - \frac{\epsilon}{\Delta x} \rho_w \frac{\left[r_w^{a+1} - (r_i + b)^{a+1}\right]}{(a+1)} + \epsilon \rho_w r_w^a \frac{dr_w}{dx}$$

$$G_2^* = G_2 - ab^2 \frac{\epsilon}{\Delta x} \int_0^1 S_{4z_2}\, y\,dy - \frac{ab^2}{\Delta x} \int_0^1 S_{4z_2}\, dy - \epsilon_c \rho_c r_c^a \frac{dr_c}{dx}$$

$$G_3^* = G_3 - ab^2 \frac{\epsilon}{\Delta x} \int_0^1 S_{4z_3}\, y\,dy - \frac{\epsilon r_i^a b}{\Delta x} \int_0^1 S_{4z_3}\, dy$$

$$G_4^* = G_4$$

$$G_5^* = G_5$$

$$G_6^* = ab^2 \int_0^1 S_{2z_6}\, y\,dy + r_i^a b \int_0^1 S_{2z_6}\, dy - ab^2 \frac{\epsilon}{\Delta x} \int_0^1 S_{4z_6}\, y\,dy - r_i^a b \frac{\epsilon}{\Delta x} \int_0^1 S_{4z_6}\, dy$$
$$+ \frac{\left(r_w^{a+1} - r_c^{a+1}\right)}{(a+1)} + \frac{\left[r_w^{a+1} - (r_i + b)^{a+1}\right]}{(a+1)} u_w^2 \frac{\partial \rho_w}{\partial p} + \frac{\left[r_i^{a+1} - r_c^{a+1}\right]}{(a-1)} \frac{d}{dp}\left(\rho_j u_j^2\right)$$

$$G_7^* = G_6 - \frac{1}{\Delta x}\left[\int_{r_i}^{r_w} \sigma\, r^a\, dr\right]_{\ell}$$

$$H_1^* = H_1 - ab^2 \frac{\epsilon}{\Delta x} \int_0^{1/2} S_{4z_1}\, y\,dy - r_i^a b \frac{\epsilon}{\Delta x} \int_0^{1/2} S_{4z_1}\, dy + \frac{1}{2} \epsilon \rho_m r_m^a \left(dr_m/dx\right)_{\ell}$$

$$H_2^* = H_2 - ab^2 \frac{\epsilon}{\Delta x} \int_0^{1/2} S_{4z_2}\, y\,dy - r_i^a b \frac{\epsilon}{\Delta x} \int_0^{1/2} S_{4z_2}\, dy - \epsilon_c \rho_c r_c^a \frac{dr_c}{dx}$$

$$H_3^* = H_3 - ab^2 \frac{\epsilon}{\Delta x} \int_0^{1/2} S_{4z_3}\, y\,dy - r_i^a b \frac{\epsilon}{\Delta x} \int_0^{1/2} S_{4z_3}\, dy$$

$$H_4^* = H_4$$

$$H_5^* = H_5$$

$$H_6^* = ab^2 \int_0^{1/2} S_{2z_6}\, y\,dy + r_i^a b \int_0^{1/2} S_{2z_6}\, dy - u_m ab^2 \int_0^{1/2} S_{1z_6}\, y\,dy - u_m r_i^a b \int_0^{1/2} S_{1z_6}\, dy$$
$$- ab^2 \frac{\epsilon}{\Delta x} \int_0^{1/2} S_{4z_6}\, y\,dy - \frac{\epsilon}{\Delta x} r_i^a b \int_0^{1/2} S_{4z_6}\, dy + \frac{\left(r_i^{a+1} - r_c^{a+1}\right)}{(a+1)} \frac{d}{dp}\left(\rho_j u_j\right)$$
$$- u_m \frac{\left(r_i^{a+1} - r_c^{a+1}\right)}{(a+1)} \frac{d}{dp}\left(\rho_j u_j\right) + \left(\frac{r_m^{a+1} - r_c^{a+1}}{a+1}\right) + \frac{1}{2} \epsilon \rho_m r_m^a \left(dr_m/dx\right)_{\ell} \frac{\partial u_c}{\partial p}$$
$$+ \frac{\epsilon}{\Delta x} ab^2 \int_0^{1/2} S_{4z_7}\, y\,dy + \frac{\epsilon}{\Delta x} r_i^a b \int_0^{1/2} S_{4z_7}\, dy$$

$$H_7^* = H_6 - \frac{1}{\Delta x}\left[\int_{r_i}^{r_m} \sigma r^a \, dr\right]_{\ell}$$

$$I_1^* = I_1 - \frac{\epsilon}{\Delta x} ab^2 \int_0^1 S_{5z_1} \, ydy - \frac{\epsilon}{\Delta x} r_i^a b \int_0^1 S_{5z_1} \, dy - \epsilon_c \rho_c r_c^a \frac{dr_c}{dx} \frac{\partial C_c}{\partial u_w}$$

$$I_2^* = I_2 - \frac{\epsilon}{\Delta x} ab^2 \int_0^1 S_{5z_2} \, ydy - \frac{\epsilon}{\Delta x} r_i^a b \int_0^1 S_{5z_2} \, dy - \epsilon_c \rho_c r_c^a \frac{dr_c}{dx} \frac{\partial C_c}{\partial u_c}$$

$$I_3^* = I_3 - \frac{\epsilon}{\Delta x} ab^2 \int_0^1 S_{5z_3} \, ydy - \frac{\epsilon}{\Delta x} r_i^a b \int_0^1 S_{5z_3} \, dy$$

$$I_4^* = I_4 - \frac{\epsilon}{\Delta x} ab^2 \int_0^1 S_{5z_4} \, ydy - \frac{\epsilon}{\Delta x} r_i^a b \int_0^1 S_{5z_4} \, dy - \epsilon_c \rho_c r_c^a \frac{dr_c}{dx} \frac{\partial C_c}{\partial C_w}$$
$$- \frac{\epsilon}{\Delta x} \rho_w \frac{\left[r_w^{a+1} - (r_i + b)^{a+1}\right]}{(a+1)} + \epsilon \rho_w r_w^a \frac{dr_w}{dx}$$

$$I_5^* = I_5 - \frac{\epsilon}{\Delta x} ab^2 \int_0^1 S_{5z_5} \, ydy - \frac{\epsilon}{\Delta x} r_i^a b \int_0^1 S_{5z_5} \, dy - \epsilon_c \rho_c r_c^a \frac{dr_c}{dx} \frac{\partial C_c}{\partial K}$$

$$I_6^* = ab^2 \int_0^1 S_{3z_6} \, ydy + r_i^a b \int_0^1 S_{3z_6} \, dy + \frac{\left(r_i^{a+1} - r_c^{a+1}\right)}{(a+1)} \frac{d}{dp} (\rho_j u_j) + \frac{\left[r_w^{a+1} - (r_i + b)^{a+1}\right]}{(a+1)}$$
$$\times \left[u_w C_w \frac{\partial \rho_w}{\partial p} - \frac{\epsilon}{\Delta x} ab^2 \int_0^1 S_{5z_6} \, ydy - \frac{\epsilon}{\Delta x} r_i^a b \int_0^1 S_{5z_6} \, dy - \epsilon_c \rho_c r_c^a \frac{dr_c}{dx} \frac{\partial C_c}{\partial p} \right.$$

$$I_7^* = I_6 - \frac{1}{\Delta x}\left[\int_{r_i}^{r_w} \beta r^a \, dr\right]_{\ell} + \frac{\epsilon}{\Delta x} ab^2 \int_0^1 S_{5z_7} \, ydy + \frac{\epsilon}{\Delta x} r_i^a b \int_0^1 S_{5z_7} \, dy$$

$$J_1^* = J_1 - \frac{\epsilon}{\Delta x} ab^2 \int_0^{1/2} S_{5z_1} \, ydy - \frac{\epsilon}{\Delta x} r_i^a b \int_0^{1/2} S_{5z_1} \, dy - \epsilon_c \rho_c r_c^a \frac{dr_c}{dx} \frac{\partial C_c}{\partial u_w} + \epsilon \rho_m r_m^a \left(\frac{dr_m}{dx}\right)_{\ell} \frac{\partial C_m}{\partial u_w}$$

$$J_2^* = J_2 - \frac{\epsilon}{\Delta x}\, ab^2 \int_0^{1/2} S_{5z_2}\, ydy - \frac{\epsilon}{\Delta x}\, r_i^a b \int_0^{1/2} S_{5z_2}\, dy - \epsilon_c \rho_c r_c^a \frac{dr_c}{dx} \frac{\partial C_c}{\partial u_c} - \epsilon \rho_m r_m^a \left(\frac{dr_m}{dx}\right)_{\ell} \frac{\partial C_m}{\partial u_c}$$

$$J_3^* = J_3 - \frac{\epsilon}{\Delta x}\, ab^2 \int_0^{1/2} S_{5z_3}\, ydy - \frac{\epsilon}{\Delta x}\, r_i^a b \int_0^{1/2} S_{5z_3}\, dy$$

$$J_4^* = J_4 - \frac{\epsilon}{\Delta x}\, ab^2 \int_0^{1/2} S_{5z_4}\, ydy - \frac{\epsilon}{\Delta x}\, r_i^a b \int_0^{1/2} S_{5z_4}\, dy - \epsilon \rho_m r_m^a \left(\frac{dr_m}{dx}\right)_{\ell} \frac{\partial C_m}{\partial C_w}$$

$$J_5^* = J_5 - \frac{\epsilon}{\Delta x}\, ab^2 \int_0^{1/2} S_{5z_5}\, ydy - \frac{\epsilon}{\Delta x}\, r_i^a b \int_0^{1/2} S_{5z_5}\, dy - \epsilon_c \rho_c r_c^a \frac{dr_c}{dx} \frac{\partial C_c}{\partial K} + \epsilon \rho_m r_m^a \left(dr_m/dx\right)_{\ell} \frac{\partial C_m}{\partial K}$$

$$J_6^* = ab^2 \int_0^{1/2} S_{3z_6}\, ydy + r_i^a b \int_0^{1/2} S_{3z_6}\, dy - C_m\, ab^2 \int_0^{1/2} S_{1z_6}\, ydy - C_m r_i^a b \int_0^{1/2} S_{1z_6}\, dy - \frac{\epsilon}{\Delta x}\, ab^2 \int_0^{1/2} S_{5z_6}\, ydy - \frac{\epsilon}{\Delta x}\, r_i^a b \int_0^{1/2} S_{5z_6}\, dy + \frac{\left[r_i^{a+1} - r_c^{a+1}\right]}{(a+1)} \frac{d}{dp}\left(\rho_j u_j\right) - C_m \frac{\left[r_i^{a+1} - r_c^{a+1}\right]}{(a+1)} \frac{d}{dp}\left(\rho_j u_j\right) - \epsilon_c \rho_c r_c^a \frac{dr_c}{dx} \frac{\partial C_c}{\partial p} + \epsilon \rho_m r_m^a \left(dr_m/dx\right)_{\ell} \frac{\partial C_m}{\partial p}$$

$$J_7^* = J_6 - \frac{1}{\Delta x} \left[\int_{r_i}^{r_m} \beta r^a dr\right]_{\ell} + \frac{\epsilon}{\Delta x}\, ab^2 \int_0^{1/2} S_{5z_7}\, ydy - \frac{\epsilon}{\Delta x}\, r_i^a b \int_0^{1/2} S_{5z_7}\, dy$$

$$L_1^* = \rho_w u_w - \frac{\epsilon}{\Delta x}\, \rho_w$$

$$L_2^* = 0$$

$$L_3^* = 0$$

$$L_4^* = 0$$

$$L_5^* = 0$$

$$L_6^* = 1.0$$

$$L_7^* = -\frac{1}{\Delta x}\left[\rho_w \epsilon \frac{du_w}{dx}\right]_{\ell}$$

In the first-wake regime (where $C_c = 1$ and $\epsilon_c = 0$), $z_1 = u_w$, $z_2 = r_i$, $z_3 = b$, $z_4 = C_w$, $z_5 = K$, $z_6 = p$, and $z_7 = x$. In addition,

$$\partial u/\partial x = 0$$

$$\frac{\partial C}{\partial u_w} = \frac{\partial C}{\partial u_c} = \frac{\partial C}{\partial p} = \frac{\partial C}{\partial x} = 0$$

$$\frac{\partial C_m}{\partial u_w} = \frac{\partial C_m}{\partial u_c} = \frac{\partial C_m}{\partial p} = 0$$

In the second-wake regime (where $r_i = r_c$ and $\epsilon_c = \epsilon$), $z_1 = u_w$, $z_2 = u_c$, $z_3 = b$, $z_4 = C_w$, $z_5 = K$, $z_6 = p$, and $z_7 = x$.

The coefficients (F*, G*, H*, I*, J*) in the third- and first-wall regime are:

$$F_1^* = F_1$$

$$F_2^* = F_2$$

$$F_3^* = F_3$$

$$F_4^* = F_4$$

$$F_5^* = F_6$$

$$F_6^* = F_6$$

$$G_1^* = G_1 - \alpha b^2 \frac{\epsilon}{\Delta x}\int_0^1 S_{4z_1}\, y\,dy - r_i^{\alpha} b \frac{\epsilon}{\Delta x}\int_0^1 S_{4z_1}\, dy + \epsilon \rho_w r_w^{\alpha} \frac{dr_w}{dx}$$

$$G_2^* = G_2 - ab^2 \frac{\epsilon}{\Delta x} \int_0^1 S_{4z_2}\, y\,dy - r_i^a b \frac{\epsilon}{\Delta x} \int_0^1 S_{4z_2}\, dy - \epsilon_c \rho_c r_c^a \frac{dr_c}{dx}$$

$$G_3^* = G_3 - \frac{\epsilon}{\Delta x} ab^2 \int_0^1 S_{4z_3}\, y\,dy - \frac{\epsilon}{\Delta x} r_i^a b \int_0^1 S_{4z_3}\, dy$$

$$G_4^* = G_4$$

$$G_5^* = G_5$$

$$G_6^* = G_6 + \frac{\epsilon}{\Delta x} ab^2 \int_0^1 S_{4z_6}\, y\,dy + \frac{\epsilon}{\Delta x} r_i^a b \int_0^1 S_{4z_6}\, dy - \frac{1}{\Delta x} \left[\int_{r_i}^{r_w} \sigma r^a\, dr \right] \ell$$

$$H_1^* = H_1 - ab^2 \frac{\epsilon}{\Delta x} \int_0^{1/2} S_{4z_1}\, y\,dy - r_i^a b \frac{\epsilon}{\Delta x} \int_0^{1/2} S_{4z_1}\, dy + \frac{1}{2} \epsilon \rho_m r_m^a \frac{dr_m}{dx}$$

$$H_2^* = H_2 - ab^2 \frac{\epsilon}{\Delta x} \int_0^{1/2} S_{4z_2}\, y\,dy - r_i^a b \frac{\epsilon}{\Delta x} \int_0^{1/2} S_{4z_2}\, dy - \frac{\epsilon}{2} \rho_m r_m^a \frac{dr_m}{dx} - \epsilon_c \rho_c r_c^a \frac{dr_c}{dx}$$

$$H_3^* = H_3 - \frac{\epsilon}{\Delta x} ab^2 \int_0^{1/2} S_{4z_3}\, y\,dy - \frac{\epsilon}{\Delta x} r_i^a b \int_0^{1/2} S_{4z_3}\, dy - \frac{\epsilon}{2} \rho_m r_m^a \frac{dr_m}{dx} \frac{\partial u_c}{\partial p}$$

$$H_4^* = H_4$$

$$H_5^* = H_5$$

$$H_6^* = H_6 + \frac{\epsilon}{\Delta x} ab^2 \int_0^{1/2} S_{4z_6}\, y\,dy + \frac{\epsilon}{\Delta x} r_i^a b \int_0^{1/2} S_{4z_6}\, dy - \frac{1}{\Delta x} \left[\int_{r_i}^{r_m} \sigma r^a\, dr \right] \ell$$

$$I_1^* = I_1 - \frac{\epsilon}{\Delta x} ab^2 \int_0^1 S_{5z_1}\, y\,dy - \frac{\epsilon}{\Delta x} r_i^a b \int_0^1 S_{5z_1}\, dy - \epsilon_c \rho_c r_c^a \frac{dr_c}{dx} \frac{\partial C_c}{\partial u_w}$$

$$I_2^* = I_2 - \frac{\epsilon}{\Delta x}\, ab^2 \int_0^1 S_{5z_2}\, y\,dy - \frac{\epsilon}{\Delta x}\, r_i^a b \int_0^1 S_{5z_2}\, dy - \epsilon_c \rho_c r_c^a \frac{dr_c}{dx} \frac{\partial C_c}{\partial u_c}$$

$$I_3^* = I_3 - \frac{\epsilon}{\Delta x}\, ab^2 \int_0^1 S_{5z_3}\, y\,dy - \frac{\epsilon}{\Delta x}\, r_i^a b \int_0^1 S_{5z_3}\, dy - \epsilon_c \rho_c r_c^a \frac{dr_c}{dx} \frac{\partial C_c}{\partial p}$$

$$I_4^* = I_4 - \frac{\epsilon}{\Delta x}\, ab^2 \int_0^1 S_{5z_4}\, y\,dy - \frac{\epsilon}{\Delta x}\, r_i^a b \int_0^1 S_{5z_4}\, dy + \epsilon \rho_w r_w^a \frac{dr_w}{dx} - \epsilon_c \rho_c r_c^a \frac{dr_c}{dx} \frac{\partial C_c}{\partial C_w}$$

$$I_5^* = I_5 - \frac{\epsilon}{\Delta x}\, ab^2 \int_0^1 S_{5z_5}\, y\,dy - \frac{\epsilon}{\Delta x}\, r_i^a b \int_0^1 S_{5z_5}\, dy - \epsilon_c \rho_c r_c^a \frac{dr_c}{dx} \frac{\partial C_c}{\partial K}$$

$$I_6^* = I_6 + \frac{\epsilon}{\Delta x}\, ab^2 \int_0^1 S_{5z_6}\, y\,dy + \frac{\epsilon}{\Delta x}\, r_i^a b \int_0^1 S_{5z_6}\, dy - \frac{1}{\Delta x} \left[\int_{r_c}^{r_w} \beta r^a\, dr \right]_\ell$$

$$J_1^* = J_1 - \frac{\epsilon}{\Delta x}\, ab^2 \int_0^1 S_{5z_1}\, y\,dy - \frac{\epsilon}{\Delta x}\, r_i^a b \int_0^1 S_{5z_1}\, dy + \epsilon \rho_m r_m^a \frac{dr_m}{dx} \frac{\partial C_m}{\partial u_w} - \epsilon \rho_c r_c^a \frac{dr_c}{dx} \frac{\partial C_c}{\partial u_w}$$

$$J_2^* = J_2 - \frac{\epsilon}{\Delta x}\, ab^2 \int_0^{1/2} S_{5z_2}\, y\,dy - \frac{\epsilon}{\Delta x}\, r_i^a b \int_0^{1/2} S_{5z_2}\, dy - \epsilon \rho_m r_m^a \frac{dr_m}{dx} \frac{\partial C_m}{\partial u_c} - \epsilon_c \rho_c r_c^a \frac{dr_c}{dx} \frac{\partial C_c}{\partial u_c}$$

$$J_3^* = J_3 - \frac{\epsilon}{\Delta x}\, ab^2 \int_0^{1/2} S_{5z_3}\, y\,dy - \frac{\epsilon}{\Delta x}\, r_i^a b \int_0^{1/2} S_{5z_3}\, dy + \epsilon \rho_m r_m^a \frac{dr_m}{\partial x} \frac{\partial C_m}{\partial p} - \epsilon_c \rho_c r_c^a \frac{dr_c}{dx} \frac{\partial C_c}{\partial p}$$

$$J_4^* = J_4 - \frac{\epsilon}{\Delta x}\, ab^2 \int_0^{1/2} S_{5z_4}\, y\,dy - \frac{\epsilon}{\Delta x}\, r_i^a b \int_0^{1/2} S_{5z_4}\, dy + \epsilon \rho_m r_m^a \frac{dr_m}{dx} \frac{\partial C_m}{\partial C_w} - \epsilon_c \rho_c r_c^a \frac{dr_c}{dx} \frac{\partial C_m}{\partial C_w}$$

$$J_5^* = J_5 - \frac{\epsilon}{\Delta x} a b^2 \int_0^{1/2} S_{5z_5} y dy - \frac{\epsilon}{\Delta x} r_i^a b \int_0^{1/2} S_{5z_5} dy$$

$$+ \epsilon \rho_m r_m^a \frac{dr_m}{dx} \frac{\partial C_m}{\partial K} - \epsilon_c \rho_c r_c^a \frac{dr_c}{dx} \frac{\partial C_c}{\partial K}$$

$$J_6^* = J_6 + \frac{\epsilon}{\Delta x} a b^2 \int_0^{1/2} S_{5z_6} y dy + \frac{\epsilon}{\Delta x} r_i^a b \int_0^{1/2} S_{5z_6} dy - \frac{1}{\Delta x} \left[\int_{r_i}^{r_m} \beta r^a dr \right]_\ell$$

In the third regime (where $r_i = r_c$ and $b = r_w - r_c$), $z_1 = u_w$, $z_2 = u_c$, $z_3 = p$, $z_4 = C_w$, $z_5 = K$, and $z_6 = x$. In addition, $\epsilon_c = \epsilon$ and $\partial u/\partial p = \partial u_c/\partial p = 0$.

In the first-wall regime (where $b = r_w - r_i$, $C_c = 1$, and $\epsilon_c = 0$), $z_1 = u_w$, $z_2 = r_i$, $z_3 = p$, $z_4 = C_w$, $z_5 = K$, and $z_6 = x$. In addition,

$$\frac{\partial C_c}{\partial u_w} = \frac{\partial C_c}{\partial p} = 0$$

$$\frac{\partial C_m}{\partial u_w} = \frac{\partial C_m}{\partial u_c} = \frac{\partial C_m}{\partial r_i} = \frac{\partial C_m}{\partial p} = 0$$

NOMENCLATURE

b	Shear layer thickness
C	Element fraction of primary stream gas
C_t	Curtet number
c	Constant in Eq. (56)
c_{fw}	Wall skin friction coefficient
c_p	Specific heat at constant pressure
F,G,H,I,J	Coefficients in system of ordinary differential equations for basic analysis
F*,G*,H*, I*,J*,L*	Coefficients in system of ordinary differential equations for extended analysis
FSP	Front stagnation point
H	Stagnation enthalpy, including chemical heats of formation
k	Eddy viscosity coefficient
k_o	Eddy viscosity coefficient for constant-density flow
K	Parameter in species profile equation
ℓ	Turbulent length scale
M_m	Mach number at half-radius control surface
N	Generalized coefficient in system of ordinary differential equations
p	Static pressure
q	Lateral turbulent species flux
r	Lateral coordinate
r_c	Lateral distance from centerline to centerbody surface
r_i	Lateral distance from centerline to inner edge of shear layer
r_m	Lateral distance from centerline to half-radius control surface

r_n	Primary nozzle exit radius
r_w	Lateral distance from centerline to duct wall
R	Gas constant
RSP	Rear stagnation point
S	Generalized integrand (Appendixes)
S_{ct}	Turbulent Schmidt number
T_o	Total temperature
u	Axial velocity component
u_k	Characteristic velocity defined by Eq. (31a)
u'	Turbulent velocity scale
v	Lateral velocity component
x	Axial coordinate
Δx	Integration step size
y	Dimensionless mixing zone coordinate (Appendixes)
$z_1 z_2 ... z_k$	Generalized dependent variable (Appendixes)
a	Geometric parameter (one for axisymmetric flow, zero for planar flow)
β	Turbulent species flux in axial direction
δ	Numerical factor used in the appendixes ($\delta = 0$ where pressure is constant, $\delta = 1$ when pressure is variable)
ϵ	Turbulent eddy viscosity
ρ	Density
σ	Turbulent normal stress in axial direction
τ	Turbulent shear stress

SUBSCRIPTS

1	Conditions in plane of primary nozzle exit
a	Conditions in isentropic secondary flow
c	Conditions at centerline or at centerbody surface
j	Conditions in isentropic primary flow
ℓ	Indicates a quantity evaluated at last upstream computation station
m	Conditions at half-radius control surface
w	Conditions at duct wall